Research Square

Preprints are preliminary reports that have not undergone peer review.
They should not be considered conclusive, used to inform clinical practice,
or referenced by the media as validated information.

Threshold-Dependent Electric Field Responses in CL-20/4,5-MDNI Cocrystals Driven by Stoichiometric Ratio

yuqin Chu
Nanjing Tech University
peng Zhang
Nanjing Tech University
yang Zhu
Nanjing Tech University
peng Ma
mapeng@njtech.edu.cn
Nanjing Tech University
Congming Ma
Nanjing Tech University

Research Article

Keywords: CL-20/4,5-MDNI cocrystal, external electric field, stoichiometric ratio, low-sensitivity energetic material

Posted Date: May 4th, 2026

DOI: https://doi.org/10.21203/rs.3.rs-9422531/v1

License: This work is licensed under a Creative Commons Attribution 4.0 International License.
Read Full License

Additional Declarations: No competing interests reported.

Threshold-Dependent Electric Field Responses in CL-20/4,5-MDNI Cocrystals Driven by Stoichiometric Ratio

Yuqin Chu, Peng Zhang, Yang Zhu, Peng Ma *, Congming Ma*
College of Safety Science and Engineering, Nanjing Tech University, Nanjing, 210009, China
*Corresponding author: Peng Ma (mapeng@njtech.edu.cn 15261877181); Congming Ma(6390@njtech.edu.cn 15950568027);

Abstract

Context: to regulate the performance of CL-20, density functional theory and molecular simulations were used to systematically investigate 1:1 and 1:3 CL-20/4,5-MDNI cocrystals under external electric fields. Molecular-level calculations were performed within −0.010 to +0.010 a.u., and crystal-level computations within 0 to +0.010 a.u.

Results show that external electric fields effectively regulate the N–NO_2 trigger bond length and sensitivity. The 1:1 cocrystal exhibits a monotonic response, while the 1:3 cocrystal shows a non-monotonic threshold response with low sensitivity only in a specific field range. Hydrogen bond analysis indicates that only C–H…O bonds exist in the 1:1 cocrystal, while both C–H…O and C–H…N bonds exist in the 1:3 cocrystal. The electric field polarizes and strengthens the hydrogen bond network, dominating the stability and sensitivity difference.Electrostatic potential and dipole moment analyses reveal monotonic charge separation in the 1:1 cocrystal and a distinct threshold response in the 1:3 cocrystal. The frontier orbital energy gap decreases monotonically with increasing electric field, with the highest stability at zero field.This study clarifies the synergistic mechanism of stoichiometric ratio, hydrogen bond network, and external electric field in CL-20-based cocrystals, supporting the design of high-efficiency and low-sensitivity energetic materials.

Methods: density functional theory (DFT) and molecular simulation were adopted. The $Dmol^3$ module in Materials Studio was used to build 1:1 and 1:3 CL-20/4,5-MDNI cocrystal models, with structural optimization and property calculation performed via PBE functional, GGA method, Grimme's DFT-D dispersion correction and DND basis set (SCF convergence criterion: 1.0×10^{-5} eV). Gaussian 16 was applied to optimize cocrystal structures with/without external electric field using B3LYP-D3/6-311+G(d,p), and M062X-D3/ma-def2-TZVPP was used for single point energy calculation. Wave function analysis was conducted with Multiwfn and VMD. Molecular-level calculations were performed within the range of −0.010 to +0.010 a.u. with a step size of 0.0025 a.u., while crystal-level computations were carried out within 0 to +0.010 a.u. with a step size of 0.001 a.u.

Keywords： CL-20/4,5-MDNI cocrystal; external electric field; stoichiometric ratio; low-sensitivity energetic material

1. Introduction

As the core power support, energetic materials are the key to achieve long-range efficient damage and precision strike capability of weapons and equipment. To enhance the safety performance and destructiveness of modern weapon systems, the development of insensitive explosives has always been a research hotspot around the world [1-4]. As a cage-type high-energy material, CL-20 is considered to be one of the most powerful explosives at present [5], but its disadvantages such as high mechanical sensitivity and easy transition to other crystal forms limit its application[6-7]. As an effective modification method, cocrystal technology has increasingly drawn scholarly attention in the domain of high-energy materials over the past few years[8]. A practical strategy for reducing the pronounced mechanical sensitivity of CL-20 is its cocrystallization with insensitive ligand molecules. This approach leverages the co-dissolution of the components in a shared solvent, where controlled precipitation under specific conditions promotes self-assembly into a composite crystal lattice stabilized by intermolecular forces [9]. The resulting supramolecular entity exhibits a unique crystal structure and tailored properties [10-11], as demonstrated by recent work on the CL-20/1-methyl-4,5-dinitroimidazole (4,5-MDNI) cocrystal. 4,5-MDNI is a diazole polynitro compound, which has been widely studied as a carrier of molten explosives, and its explosive performance is better than TNT[9]. The cocrystal formed by the molecular structure of CL-20 and 4,5-MDNI exhibits high density, superior detonation performance, low impact sensitivity, and excellent thermal stability for the cocrystal and excellent comprehensive performance, which has high research value [6]. **Fig.1** briefly illustrates the synthesis routes of 1:1 and 1:3 CL-20/4,5-MDNI cocrystals. Tan et al. [12] successfully synthesized the 1:3 CL-20/4,5-MDNI cocrystal and validated its static low sensitivity, yet they neglected to explore the cocrystal's dynamic responses to external electric fields. Consequently, their work lacked theoretical backing for the "targeted sensitivity modulation" required in engineering applications.The subsequent research of Yang et al. [12] further verified the structural stability and performance adjustability of this kind of cocrystal, which provided theoretical references for the customized design of energetic cocrystals.

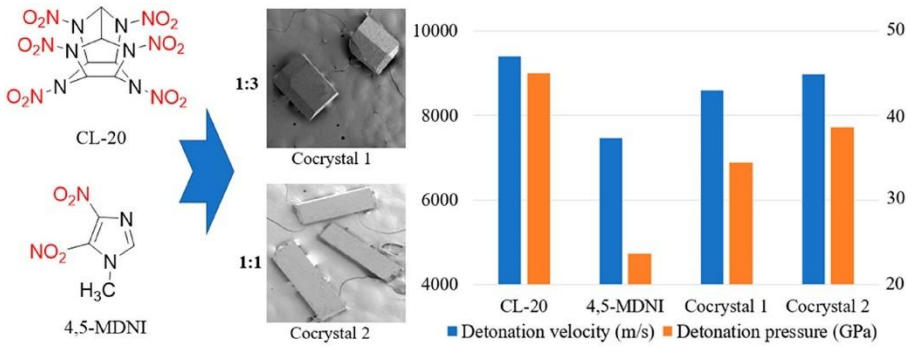

Fig.1 Synthesis of 1:1CL-20/4,5MDNI and 1:3 CL-20/4,5MDNcocrystals

In the research on the reaction process of energetic materials, scholars used to focus on mechanical action and high temperature action [13-17], and paid less attention to the effects of external electric field modulation However, studies have shown that the external electric field can change the molecular structure, thereby affecting the performance of energetic materials (such as sensitivity) [18-21]. Zhang et al. [22] Investigated the response behaviors of ICM series explosives (ICM-101,ICM-102,ICM-103) under external electric, and found that the increase of electric field intensity can reduce the HOMO-LUMO energy gap and reduce the electron localization function (ELF), resulting in the easy fracture of trigger bond and the increase of sensitivity. Liu et al. [23] used the first-principles calculation method to investigate the modulation mechanism by which external electric fields regulate the sensitivity of β-HMX explosives across the dual scales of molecule and crystal. but their work focused on single-component systems and did not involve the synergistic response of hydrogen bond networks and electronic structures in cocrystal systems, making it difficult to clarify the microcosmic mechanism of electric field regulation. Ren et al. [24] found that the externally applied electric field exerts a notable regulatory effect on the N-O bond in CH_3NO_2 molecule and the N-N bond in NH_2NO_2 molecule, and may change the decomposition reaction path of the molecule, and ultimately affect the detonation velocity, detonation pressure and sensitivity level of such substances. A series of studies by Politzer et al. [25-26] confirmed that the molecular polarity and charge distribution of Typical energetic materials exemplified by HMX and RDX can be directionally regulated by the magnitude and direction of the externally applied electric field which provides a new idea for the precise regulation of sensitivity and energy release efficiency. In addition, Hao et al. [27] investigated the external electric field response of CL-20/BTF 1:1 cocrystals and observed linear variations in N-NO_2 bond lengths. Nevertheless, they did not examine how stoichiometric ratios affect response patterns, rendering them unable to account for the stability discrepancies among multi-ratio cocrystals.

External electric field can induce changes in molecular structure, thereby affecting its sensitivity and other specific properties, which has been confirmed in many previous studies[18-21]. Specifically, some studies have pointed out that electric fields with different intensities and directions exert a notable impact on the structural features and performance of various high-energy molecules[28-29]. Other research findings have indicated that the externally applied electric field can polarize organic molecules, thereby promoting ionization and participating in chemical reactions[30-31]. In addition, The externally applied electric field also exerts a notable impact on the trigger bonds of high-energy molecules, which may change the decomposition reaction process and sensitivity of energetic materials. These research results fully reveal the far-reaching impact of externally imposed electric fields on energetic molecules. Although extensive research on the properties and theoretical investigations of single-ratio CL-20/4,5-MDNI cocrystals has been conducted [32-33], how the electric field affects the intermolecular interaction and charge distribution in CL-20/4,5-MDNI cocrystals with varied stoichiometric ratios remains to be further studied.

To fill these research gaps and advance the field of energetic material performance

regulation, this study's core innovations are as follows:

For the first time, the "threshold-type response" of the N-NO_2 trigger bond and electrostatic potential in the 1:3 CL-20/4,5-MDNI cocrystal in negative electric fields is reported, which corrects the traditional cognition that "the electric field regulation of energetic cocrystals is linear" and supplements the diversity of electric field response patterns in cocrystal systems.

Stoichiometric ratio is shown to modulate cocrystals' electric field-sensitive crystal orientations ([010] for 1:1 and [001] for 1:3), identifying novel targets for directional regulation of cocrystal stability and sensitivity.

A positive correlation between hydrogen bond network density and electric field response sensitivity is established: the 1:3 cocrystal with a denser hydrogen bond network (12 bonds/unit cell) exhibits higher electric field response sensitivity than the 1:1 cocrystal (8 bonds/unit cell), providing a new structural design basis for optimizing the electric field regulation efficiency of energetic cocrystals.

Accordingly, this study explores the molecular architecture, electronic structure, and intermolecular interactions of 1:1 and 1:3 CL-20/4,5-MDNI cocrystals under 0.001–0.01 a.u. external electric fields. By revealing the synergistic regulation mechanism of stoichiometric ratio and external electric field, it offers theoretical support for performance optimization and safe application of high-energy, low-sensitivity energetic materials.

2. Calculation details

In this study, crystal models of 1:1 and 1:3 CL-20/4,5-MDNI cocrystals were con structed using the Dmol3 module in Materials Studio. Structural optimization and pro perty calculations were performed using the DMol3 program [34,35]. The Perdew–Bu rke–Ernzerhof (PBE) functional within the generalized gradient approximation (GGA) was adopted, together with Grimme's DFT-D dispersion correction [37]. The DND b asis set was employed, and the self-consistent field (SCF) convergence criterion was s et to 1.0×10^{-5} eV [36]. It has been verified that density functional theory with the PB E functional is suitable for evaluating the electronic properties of CHON-containing e nergetic materials [38]. All optimized structures were confirmed to be local energy mi nima with no imaginary vibrational frequencies. External electric fields were applied a long the [100], [010], and [001] directions at intensities from 0 to 0.01 a.u. with a step size of 0.001 a.u., and the electronic structures and intermolecular charge interactions were calculated under various field strengths. The crystal structures were obtained fro m the Cambridge Crystallographic Data Centre (CCDC) under accession numbers 197 2670 and 199369 (https://www.ccdc.cam.ac.uk/conts/Retrieval.html). This model provides the band structure, density of states (DOS), and crystal orientatio n-dependent responses as reported in Sections 3.2.4 and 3.2.5. To clearly present the s tructural characteristics of the two cocrystal systems, their crystal structures are illustr ated in **Fig.2**.

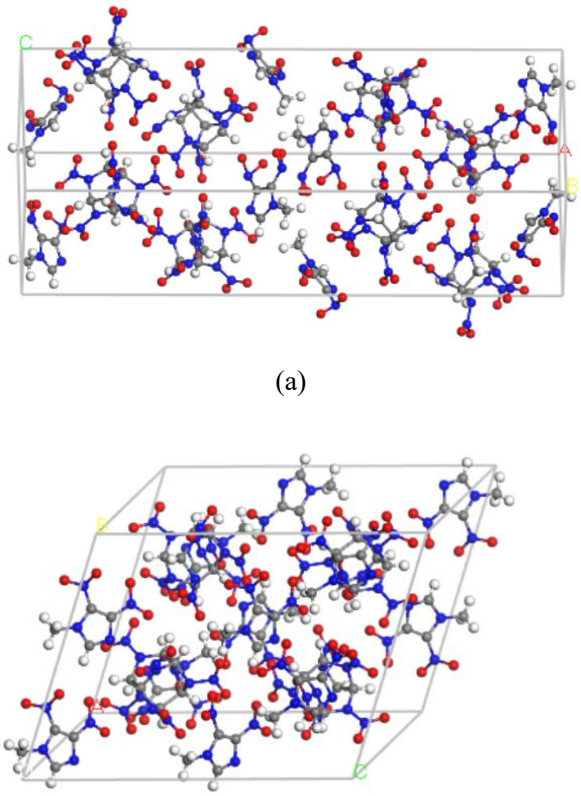

(a)

(b)

Fig.2 Crystal structure of 1:1CL-20/4,5MDNI(a)and 1:3CL-20 / 4,5MDNI(b)

Relevant computations were executed using the Gaussian 16 software package [39]. Considering that the B3LYP functional combined with D3 dispersion correction has good applicability to the molecular structure optimization of energetic materials, and the 6-311+G(d,p) basis set can precisely describe the electron distribution characteristics of light atoms, The B3LYP-D3/6-311+G(d,p) computational approach was employed to fully optimize the initial structure of the cocrystal molecule under two conditions: the presence of an external electric field and its absence. The thermodynamic stability of the cocrystal structure was evaluated based on dual criteria: "no imaginary frequencies in the calculation results" and "satisfaction of all four convergence criteria." In view of the fact that the calculation of single point energy requires more accurate electronic structure description, the M062X-D3 / ma-def2-TZVPP method (which has better calculation accuracy for intermolecularinteraction) is further selected to complete the calculation of single point energy of two different proportions of eutectic molecules. [40-41] Wave function analysis was performed using Multiwfn [42-43] and VMD [44] software. The value range of the external electric field intensity is -0.01 to 0.01 atomic units, and the increasing step size is set to 0.0025 atomic units. This model yields the trigger bond length, electrostatic potential (ESP), frontier molecular orbitals (FMO), and dipole moment presented in Sections 3.1.1, 3.2.1, 3.2.2, and 3.2.3, as well as the topological analysis of hydrogen bonds in Section 3.3.

Results and Discussion

3.1Molecular structure

3.1.1 Trigger key length

The difficulty of detonation reaction of energetic materials under external stimulation is defined as the sensitivity of such materials. For energetic material systems, the qualitative analysis of the change trend of material sensitivity can be realized by exploring the structural change law of the material's internal triggering bond. Generally, the higher the material's sensitivity magnitude, the higher the probability of detonation reaction under the action of the outside world. From the perspective of chemical structure, a trigger bond in energetic material molecules is defined as a type of chemical bond with the minimum bond order and weakest bond energy. It has been confirmed that in the trigger bond system of energetic materials, The bond length parameter and bond energy magnitude exhibit a negative correlation, that is, The greater the bond length of the triggering bond, the lower the bond energy magnitude, which leads to a significant increase in the sensitivity of energetic materials [26]. Therefore, Multiwfn [42-43] was used to analyze the two optimized molecules by Laplace (LBO) bond order analysis, Thus, it was deduced that the trigger bonds in the molecules of the two proportions are N-NO_2 bonds, which are highlighted by the boxes in the **Fig. 3**. Re Relevant research has verified that the regulatory effect of an external electric field on the trigger bond is most prominent when the field direction is parallel to the molecular orientation of this bond. With the aim of revealing how the applied electric field regulates the trigger bond of cocrystal explosives, the orientation of the positive direction of the applied electric field N → NO_2 (and the opposite direction, NO_2 → N, as the negative applied electric field) by incorporating the key bonding characteristics of N atoms and NO_2 groups. This setting matches the electron transfer path pertaining to the trigger bond for ensuring the study's rationality, and the chosen electric field intensity gradients are 0.000, ± 0.005, ± 0.0075 and ± 0.010 atomic units, covering the conventional research range, which can effectively capture the sensitive changes of bond structure.

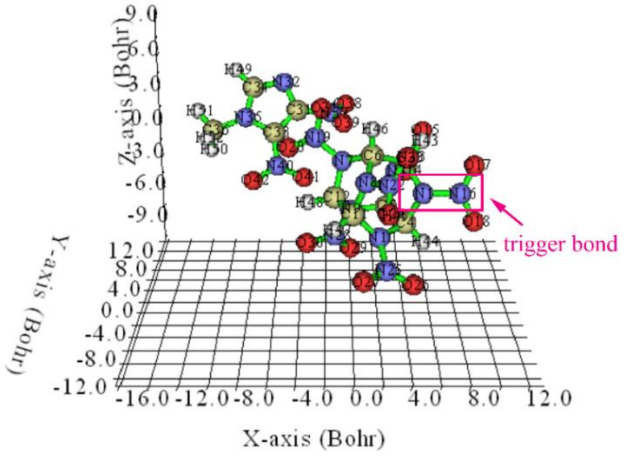

（a）

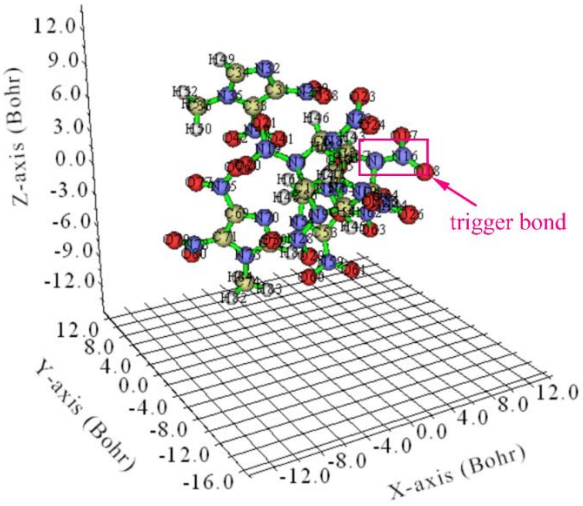

(b)

Fig.3 Direction-Adjusted Ball-Stick Model Diagram of1:1 CL-20/4,5-MDNI(a)and 1:3 CL-20/4,5-MDNI(b)

For the 1:1 system(**Table 1**), the $R_{N\text{-}NO2}$ is monotonically elongated under the positive electric field (such as the electric field varies from 0 to 0.010 a.u., the bond length expands from 1.44352 Å to 1.48309 Å), the bond energy is weakened, and the sensitivity is significantly improved. In the context of a negative electric field, the bond length monotonically shrinks (For instance, as the electric field changes from 0 to −0.010 a.u., the bond length reduces from 1.44352 Å to 1.41211 Å), the bond energy is enhanced, and the sensitivity is reduced. This linear response trend is consistent with the general law of electric field regulation on trigger bonds reported in previous studies [27,33], but the magnitude of change differs significantly. Specifically, Hao et al. [27] reported that the N-NO_2 bond length of CL-20/BTF 1:1 cocrystal increased by 0.031 Å when the electric field increased from 0 to 0.01 a.u., while the bond length increase of CL-20/4,5-MDNI 1:1 cocrystal in this study reaches 0.03957 Å. This difference arises

from the conjugated structure of the imidazole ring in 4,5-MDNI, which enhances electric field-induced charge transfer between CL-20 and 4,5-MDNI, making the N-NO_2 bond more polarizable. This finding indicates that the selection of cocrystal components can modulate the electric field regulation efficiency of trigger bonds, providing a new idea for the design of cocrystals with adjustable sensitivity.

For the 1:3 system(**Table 2**), $R_{N\text{-}NO2}$ is also monotonously elongated under the positive electric field (For instance, as the electric field varies from 0 to 0.010 a.u., the bond length expands from 1.44673 Å to 1.49654 Å), and the sensitivity increases. In the negative electric field, the bond length first shrinks and then abnormally elongates. I When the electric field is between −0.0025 and −0.0075 a.u., the bond length shortens. Take the field change from 0 to −0.0075 a.u. as an illustration: the bond length declines from 1.44673 Å to 1.42796 Å. and the sensitivity decreases. When the electric field intensity surpasses −0.0075 a.u. (e.g., at −0.010 a.u.), the bond length abnormally elongates (increases to 1.46352 Å), and the sensitivity increases again. This nonlinear response exhibits remarkable differences from the linear regulatory behavior found in the 1:1 cocrystal as well as other previously documented CL-20-based single-ratio cocrystals [27,33]. Tan et al. [12] examined the static structure of the CL-20/4,5-MDNI 1:3 cocrystal under field-free conditions and verified its superior thermal stability, yet they did not investigate the dynamic structural evolutions of this cocrystal upon exposure to external electric fields. The "threshold-type" variation of trigger bonds identified in the present work suggests that the 1:3 cocrystal features a unique electric field window corresponding to low sensitivity, a characteristic that has not been reported in prior studies. The underlying mechanism of this phenomenon lies in the superimposition of intermolecular interactions triggered by the excess 4,5-MDNI molecules in the 1:3 cocrystal: under weak negative electric fields, strengthened hydrogen bond interactions (see Section 3.3) facilitate the contraction of N-NO_2 bonds; in contrast, under strong negative electric fields, excessive polarization of the imidazole ring leads to charge redistribution, thereby inducing the elongation of trigger bonds. This discovery revises the conventional notion that "electric field regulation of energetic cocrystals is universally linear" and lays a theoretical foundation for the precise modulation of low sensitivity in the 1:3 cocrystal.

In summary, the $R_{N\text{-}NO_2}$ trigger bond's bond length can be changed by adjusting the applied electric field's orientation and intensity, and then the sensitivity of the 1 : 1 and 1 : 3 CL-20 / 4,5-MDNI systems can be controlled : the electric field with a positive orientation enhances the sensitivity to optimize the detonation performance, and the negative electric field (1:1 system can be applied in full range, 1 : 3 system needs to be controlled in the range of (− 0.0025 ~ − 0.0075a.u.) reduces the sensitivity to improve storage stability.

Table 1 Trigger Bond Lengths of 1:1 CL-20/4,5-MDNI Cocrystal Under Different External Electric Fields

External electric field/a.u.	$R_{N\text{-}NO2}$/ Å	$\triangle R_{N\text{-}NO2}$/ Å
0.010	1.48309	0.03957
0.0075	1.46773	0.02421

	0.005	1.45389	0.01037
	0.0025	1.44501	0.00149
CL-20/4,5MDNI	0.000	1.44352	0
	-0.0025	1.42871	-0.01481
	-0.005	1.41926	-0.02426
	-0.0075	1.41066	-0.03286
	-0.010	1.41211	-0.03141

Table 2 Trigger Bond Lengths of 1:3 CL-20/4,5-MDNI Cocrystal Under Different External Electric Fields

	External electric field/a.u.	$R_{N\text{-}NO2}$/ Å	$\triangle R_{N\text{-}NO2}$/ Å
	0.010	1.49654	0.04981
	0.0075	1.47549	0.02876
	0.005	1.46037	0.01364
	0.0025	1.45321	0.00648
1:3CL-20/4,5MDNI	0.000	1.44673	0
	-0.0025	1.43090	-0.01583
	-0.005	1.42796	-0.01877
	-0.0075	1.43619	-0.01054
	-0.010	1.46352	0.01679

3.1.2 The shortest distance between the molecular center of mass and the molecule

External electric fields (EEF) modulate intermolecular interactions via molecular polarization and structural rearrangement[45]. To investigate intermolecular interactions in CL-20/4,5-MDNI cocrystals, the shortest centroid distances between CL-20 and 4,5-MDNI molecules were calculated under external electric fields (EEF) along the [100], [010], and [001] directions. Changes in these distances reflect the modulation of noncovalent interactions, which are closely related to structural stability, sensitivity, and energetic properties.

For the 1:1 cocrystal (**Tables 3** and **4**), both components display distinct anisotropic responses to EEF. The most significant distance fluctuations appear along the [001] direction, and the separations along [001] are generally larger than those along [100] and [010], indicating that the [001] orientation is more sensitive to electric field regulation.

Table 3 Shortest Distances of Molecular Centroids in 1:1 CL-20 Under Varied External Electric Fields

100		010		001	
EEF/a.u.	Shortest distance/Å	EEF/a.u.	Shortest distance/Å	EEF/a.u.	Shortest distance/Å
0	1.508	0	1.508	0	1.508
0.001	1.639	0.001	1.673	0.001	1.677
0.002	1.612	0.002	1.673	0.002	1.605
0.003	1.612	0.003	1.709	0.003	1.841
0.004	1.825	0.004	1.826	0.004	2.056
0.005	1.641	0.005	1.579	0.005	1.878
0.006	1.641	0.006	1.465	0.006	1.673
0.007	1.809	0.007	1.932	0.007	2.321

0.008	1.471	0.008	1.612	0.008	1.948
0.009	1.692	0.009	1.643	0.009	1.705
0.01	1.677	0.01	1.72	0.01	1.825

Table 4 Shortest Distances of Molecular Centroids in 1:1 4,5-MDNI Under Varied External Electric Fields

100		010		001	
EEF/a.u.	Shortest distance/Å	EEF/a.u.	Shortest distance/Å	EEF/a.u.	Shortest distance/Å
0	0.609	0	0.609	0	0.609
0.001	0.607	0.001	0.603	0.001	0.694
0.002	0.607	0.002	0.876	0.002	1.312
0.003	0.841	0.003	0.632	0.003	1.113
0.004	0.601	0.004	0.705	0.004	0.97
0.005	0.846	0.005	0.732	0.005	1.871
0.006	0.842	0.006	0.694	0.006	1.213
0.007	0.609	0.007	0.568	0.007	0.820
0.008	0.612	0.008	0.783	0.008	0.761
0.009	0.837	0.009	0.656	0.009	0.672
0.01	0.610	0.01	0.509	0.01	0.793

In comparison, the 1:3 cocrystal (**Tables 5** and **6**) shows much stronger distance variations under the same EEF, particularly for CL-20 along [001] and 4,5-MDNI along [010]. The wider range of changes in the 1:3 system demonstrates that increasing 4,5-MDNI content amplifies the structural response to external electric fields. Overall, EEF effectively modulates intermolecular distances in an anisotropic and stoichiometry-dependent manner. These variations alter hydrogen-bonding and van der Waals interactions, thereby affecting molecular packing and macroscopic performance. The results provide a theoretical basis for regulating the structure and properties of CL-20/4,5-MDNI cocrystals for high-energy low-sensitivity applications.

Table 5 Shortest Distances of Molecular Centroids in 1:3 CL-20 Under Varied External Electric Fields

100		010		001	
EEF/a.u.	Shortest distance/Å	EEF/a.u.	Shortest distance/Å	EEF/a.u.	Shortest distance/Å
0	1.148	0	1.148	0	1.148
0.001	1.608	0.001	1.787	0.001	1.608
0.002	1.623	0.002	1.609	0.002	1.411
0.003	1.148	0.003	1.703	0.003	1.703
0.004	1.608	0.004	1.608	0.004	1.623
0.005	1.623	0.005	1.701	0.005	1.631
0.006	1.666	0.006	1.732	0.006	1.808
0.007	1.623	0.007	1.666	0.007	1.769
0.008	1.608	0.008	1.854	0.008	1.459
0.009	1.432	0.009	1.808	0.009	1.91
0.01	1.632	0.01	1.703	0.01	1.508

Table 6 Shortest Distances of Molecular Centroids in 1:3 4,5-MDNI Under Varied External Electric Fields

100 EEF/a.u.	Shortest distance/Å	010 EEF/a.u.	Shortest distance/Å	001 EEF/a.u.	Shortest distance/Å
0	3.805	0	3.805	0	3.805
0.001	3.74	0.001	4.349	0.001	3.612
0.002	3.805	0.002	3.813	0.002	3.612
0.003	4.349	0.003	3.612	0.003	2.517
0.004	2.566	0.004	3.612	0.004	3.612
0.005	2.566	0.005	1.411	0.005	4.057
0.006	3.612	0.006	1.54	0.006	3.74
0.007	4.349	0.007	3.805	0.007	3.74
0.008	4.364	0.008	3.74	0.008	4.074
0.009	3.612	0.009	3.612	0.009	3.612
0.01	3.805	0.01	3.805	0.01	4.109

3.2 Electronic structure

3.2.1 Electrostatic potential

Electrostatic potential refers to a physical quantity that characterizes potential energy of a point in spatial dimensions, which mirrors a unit positive charge's potential energy within the electrostatic field, In the molecular system, the electrostatic potential is the electric field's potential energy distribution generated by the charge of all nuclei and electrons in the molecule at a certain point in space. Red represents the positive region (Vmax electron-deficient, nucleophilic attack site), blue represents the negative region (Vmin electron-rich, electrophilic attack site), the extreme value of the electrostatic potential (VmaxVmin) and the distribution pattern, directly related to the molecular reactivity, polarity, sensitivity and other key properties [46].

Using Multiwfn and VMD software, the surface electrostatic potential (ESP) of the two proportional eutectic molecules under the applied electric field was calculated and plotted, as shown in the figure. The maximum and minimum values of surface ESP are listed in the table.

The electrostatic potential extremum and surface distribution of 1:1 CL-20/4,5-M DNI show a significant anisotropic response with the applied external electric field(**Ta ble 7**). Under the positive electric field (EEF>0a.u.), Vmax increases monotonically fr om 51.24 kcal / mol to 74.82 kcal/mol, and Vmin decreases monotonically from-26.92 kcal /mol to-43.69 kcal/mol. Under the negatively charged electric field (EEF< 0a.u.), Vmax increases monotonically from 51.24 kcal/mol to 75.09 kcal/mol, and Vmin dec reases monotonically from-26.92 kcal/mol to-42.83 kcal/mol. It is evident that both po sitive and negative electric fields make the molecule 's ' positive region more positive and negative region more negative ', the degree of charge separation increases as the e lectric field intensity rises, and the molecule exhibits greater sensitivity to the charge r esponse of negative electric field (e.g., the Vmax at-0.010 a.u.is higher than that at 0.0

10 a.u.). From the electrostatic potential diagram of the molecular surface (**Fig.4**), the r ed (positive region) and blue (negative region) regions gradually expand and the color deepens under the positive electric field. the red region distributes predominantly aro und the CL-20 molecule's nitro oxygen atoms and the amino hydrogen atom of 4,5-M DNI molecule. The color depth changes more notably with the application of the nega tive electric field, which further verifies the charge response sensitivity of the molecul e toward the negatively charged electric field.

Table 7 Maximum and minimum values of surface electrostatic potential of 1:1 CL-20/4,5-MDNI cocrystal molecules under different external electric fields

	External electric field/a.u.	V_{max}/kcal mol^{-1}	V_{min}/kcal mol^{-1}
CL-20/4,5MDNI	0.010	74.82	-43.69
	0.0075	68.35	-37.44
	0.005	60.08	-33.05
	0.0025	54.71	-28.56
	0.000	51.24	-26.92
	-0.0025	64.93	-29.51
	-0.005	66.84	-32.07
	-0.0075	71.86	-37.88
	-0.010	75.09	-42.83

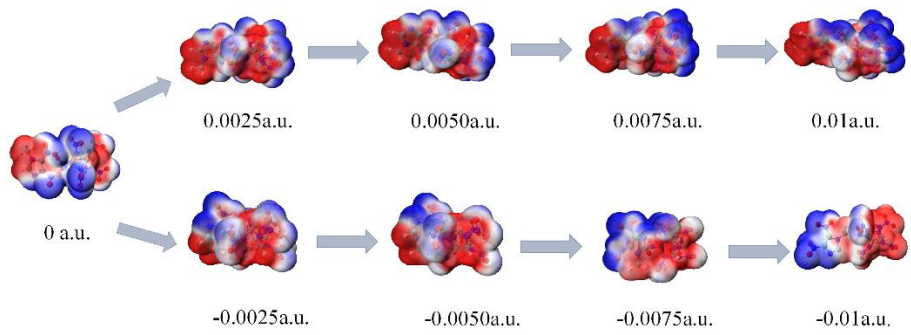

Fig.4 Electrostatic Potential Maps of 1:1 CL-20/4,5-MDNI Cocrystal Molecules Under Different External Electric Fields

For the 1:3 CL-20/4,5-MDNI composite(**Table 8**), the electrostatic potential exhibits a highly complex asymmetric and non-monotonic response to the applied external electric field: In the context of a positive-polarity electric field,Vmax decreases first from 58.07 kcal · mol^{-1} (at 0.000 a.u.) to 55.87 kcal · mol^{-1} (at 0.0025 a.u.) and then increases to 71.64 kcal · mol^{-1} (at 0.010 a.u.), showing a "first decrease then increase" trend, while Vmin decreases monotonically from -28.29 kcal · mol^{-1} to -60.82 kcal · mol^{-1}; under a negative electric field, Vmax decreases first from 58.07 kcal

· mol^{-1} (at 0.000 a.u.) to 46.97 kcal · mol^{-1} (at -0.0025 a.u.) and then increases to 72.81 kcal · mol^{-1} (at -0.010 a.u.), presenting a "first decrease then increase" pattern, and Vmin increases first from -28.29 kcal · mol^{-1} to -26.06 kcal · mol^{-1} (at -0.0025 a.u.) and then decreases to -57.54 kcal · mol^{-1} (at -0.010 a.u.), demonstrating a "first increase then decrease" behavior. The molecular surface electrostatic potential maps also visually confirm this regularity(**Fig.5**): under both positive and negative electric fields, the red and blue regions first contract briefly (corresponding to reduced sensitivity under weak electric fields) and then gradually expand with deepened colors (corresponding to increased sensitivity under strong electric fields), reflecting the "threshold-type" regulation of the electric field on the molecular surface charge distribution.

Table 8 Maximum and minimum values of surface electrostatic potential of 1:3 CL-20/4,5-MDNI cocrystal molecules under different external electric fields

	External electric field/a.u.	V_{max}/kcal mol^{-1}	V_{min}/kcal mol^{-1}
1:3CL-20/4,5-MDNI	0.010	71.64	-60.82
	0.0075	65.03	-44.25
	0.005	60.93	-38.58
	0.0025	55.87	-31.92
	0.000	58.07	-28.29
	-0.0025	46.97	-26.06
	-0.005	56.34	-33.82
	-0.0075	62.89	-50.58
	-0.010	72.81	-57.54

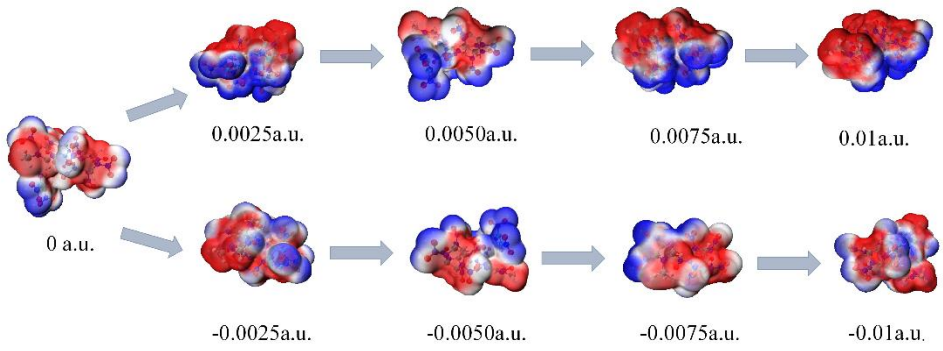

Fig.5 Electrostatic Potential Maps of 1:3 CL-20/4,5-MDNI Cocrystal Molecules Under Different External Electric Fields

3.2.2 Frontier molecular orbitals

Frontier molecular orbitals (FMOs) represent a category of molecular orbitals that exert a pivotal function in chemical reactivity in molecular orbital theory. The core

includes The highest occupied (HOMO) and lowest unoccupied (LUMO) molecular orbitals. It is the core concept to comprehend molecular chemical reactivity, electron transfer law and material properties (such as stability and responsiveness exhibited by energetic materials) [47]. HOMO (highest occupied molecular orbital) denotes the molecular orbital in a molecule that bears the greatest energy and accommodates electrons. These electrons are the ' active electrons ' that are most easily excited or transferred when molecules participate in chemical reactions. In energetic materials, the electron cloud distribution of HOMO often corresponds to the molecular region with abundant electrons (eg., groups containing amino and aromatic rings), which is an electron donor site for electrophilic reactions. LUMO (lowest unoccupied molecular orbital) denotes the molecular orbital within a molecule that has the least energy and remains unoccupied by electrons. It can be regarded as the ' lowest energy level vacancy ' of electrons in the molecule, and electrons are easily accepted in chemical reactions. In energetic materials, the electron cloud distribution of LUMO usually corresponds to the electron-deficient region (such as groups containing nitro and carbonyl groups), which is the electron acceptor site of nucleophilic reaction. The energy gap between LUMO and HOMO ($\Delta E_{LUMO-HOMO}$) (the difference between LUMO energy and HOMO energy) has a key physical meaning : The greater the energy gap, the higher the molecular stability, the lower the chemical activity, and the lower the sensitivity of energetic materials (detonation difficulty); The narrower the energy gap, the higher the molecular activity, the greater the reactivity, and the stronger the sensitivity — electron transfer thus becomes more facile [48].

Fig.6 and **Table 9** show that LUMO is primarily localized around the nitro group ($-NO_2$) in 4,5-MDNI under all electric field conditions. The HOMOs are mainly distributed in the imidazole ring (aromatic ring conjugated region) of 4,5-MDNI. When there is no electric field (0.000 a.u.), the energy gap is 4.58 eV, which is the maximum Under the full range of electric field conditions. At this time, the molecule is the most stable and the sensitivity is the lowest; as the intensity of the positive and negative electric field, the energy gap declines monotonously, and the decrease is more significant in the context of a negative-polarity electric field, this suggests that the molecular activity is increased and the sensitivity is increased. This trend aligns with Zhang et al.'s [22] report on ICM series explosives, where electric field-induced polarization narrows the HOMO-LUMO gap and boosts molecular activity. Notably, the 1:1 CL-20/4,5-MDNI cocrystal shows a larger gap reduction (2.06 eV at −0.010 a.u.) than ICM-101 (1.8 eV under the same field) [22]. This discrepancy stems from stronger intermolecular charge transfer between CL-20 and 4,5-MDNI: the conjugated structure of 4,5-MDNI's imidazole ring and nitro group facilitates electric field-driven electron delocalization, accelerating gap narrowing. This finding indicates that cocrystal engineering enhances the electric field responsiveness of energetic materials, offering a new strategy to optimize their sensitivity regulation efficiency.

Table 9 External electric field-dependent HOMO, LUMO, and band gap of1:1 CL-20/4,5-MDNI

External electric field/a.u.	HOMO	LUMO	$\Delta E_{LUMO-HOMO}$

	0.010	-6.52	-3.95	2.57
	0.0075	-7.11	-3.55	3.56
	0.005	-7.31	-3.32	3.99
	0.0025	-7.73	-3.24	4.49
CL-20/4,5MDNI	0.000	-8.61	-4.03	4.58
	-0.0025	-8.58	-4.12	4.46
	-0.005	-8.55	-4.39	4.16
	-0.0075	-8.63	-4.77	3.86
	-0.010	-8.39	-5.87	2.52

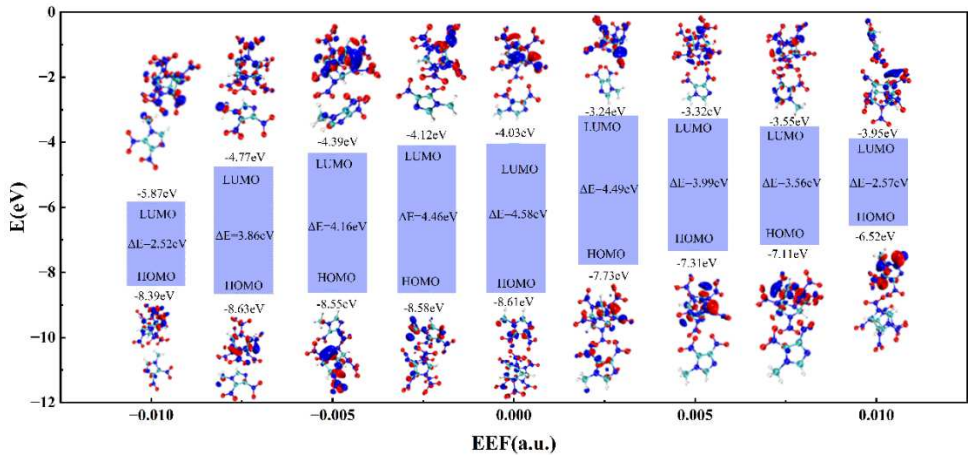

Fig.6 External electric field-dependent HOMO, LUMO, and band gap map of1:1 CL-20/4,5-MDNI

Fig.7 and **Table 10** show the HOMO and LUMO of the 1:3 CL-20/4,5-MDNI composite. The HOMO is primarily localized in the imidazole ring of 4,5-MDNI, and the LUMO is primarily localized in the nitro of 4,5-MDNI, which is consistent with the orbital distribution of the 1:1 system. When there is no electric field (0.000 a.u.), the energy gap is 4.08 eV, the molecule is the most stable and the sensitivity is the lowest. The energy gap also shows a decreasing trend as a whole. The energy gap continues to decrease from 3.99 eV to 3.23 eV as the positive electric field intensifies (0.0025→ 0.010 a.u.), meanwhile, the energy gap narrows from 3.75 eV to 3.06 eV in the context of a negative electric field. However, the value of the overall energy gap exceeds that of the 1:1 ratio system indicating that the molecules are more active and more sensitive at the 1:3ratio. This result appears contradictory to Yang et al.'s [12] conclusion that "increased 4,5-MDNI content improves cocrystal stability," a discrepancy rooted in differing research contexts. Yang et al. [12] focused on static stability under field-free conditions, where higher hydrogen bond network density (12 vs. 8 bonds/unit cell for 1:3 and 1:1 cocrystals, respectively) enhances stability. Under electric fields, however, excess 4,5-MDNI in the 1:3 cocrystal forms polar molecular clusters, strengthening HOMO-LUMO electron cloud overlap and accelerating energy gap narrowing. This study clarifies the "double-edged sword" effect of 4,5-MDNI content: it boosts static stability but enhances electric field-induced activity, revising the one-sided view that "4,5-MDNI content correlates positively with stability" and providing a more comprehensive basis for cocrystal ratio selection.

Table 10 External electric field-dependent HOMO, LUMO, and band gap of1:3 CL-20/4,5-MDNI

	External electric field/a.u.	HOMO	LUMO	$\Delta E_{LUMO-HOMO}$
1:3CL-20/4,5MDNI	0.010	-7.64	-4.41	3.23
	0.0075	-7.65	-4.06	3.59
	0.005	-7.77	-3.81	3.96
	0.0025	-7.78	-3.79	3.99
	0.000	-7.62	-3.54	4.08
	-0.0025	-7.66	-3.91	3.75
	-0.005	-7.73	-4.19	3.54
	-0.0075	-7.66	-4.41	3.25
	-0.010	-8.89	-5.83	3.06

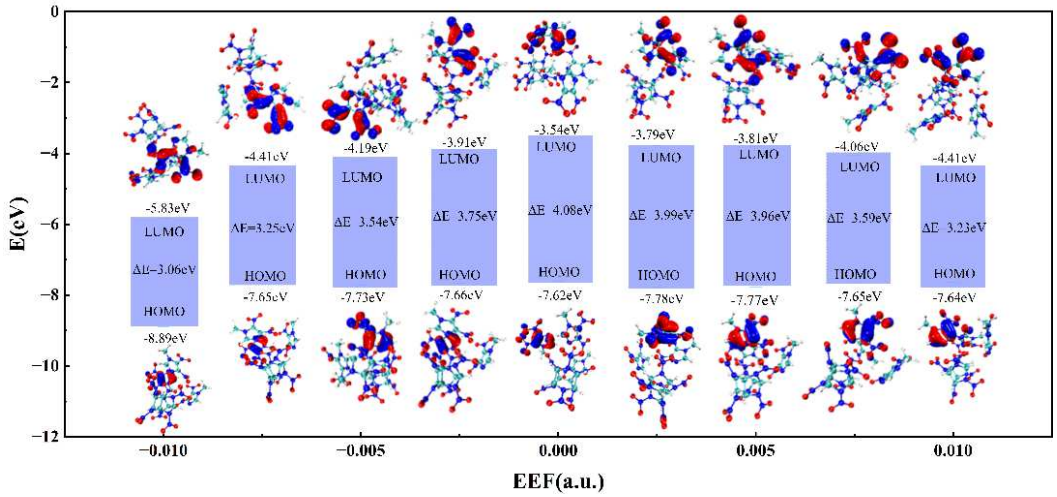

Fig.7 External electric field-dependent HOMO, LUMO, and band gap map of1:3 CL-20/4,5-MDNI

3.2.3 Dipole moment

The molecular dipole moment serves as a physical quantity describing the asymmetry of charge distribution in molecules, which is derived from the charge separation caused by the non-coincidence of the average positions of atomic nuclei and electrons in molecules. The size and direction of the dipole moment (μ=q×d) is capable of reflecting molecular polarity, (μ=0:non-polar;μ>0:polarity), which in turn affects various physical and chemical properties of the molecule. In the energetic material system, the external electric field (EEF) can induce the polarization phenomenon and realize the precise control of the dipole moment μ. [49].

The total dipole moment exhibits a ' V-shaped ' asymmetric response(**Fig.8**). (**Table 11**) In the context of a negative-polarity electric field, the total dipole moment increases from 9.6395 Debye to 21.1454 Debye with a rise in the electric field's strength and the degree of charge separation is enhanced. Under the positive electric field, it increases linearly to 22.5145 Debye with a rise in the electric field's strength, in which the X-axis component dominates and contributes more than 70%. The Y-axis component

decreases continuously from 0.2522 Debye (-0.010a.u.) to-4.0930 Debye (0a.u.), and then changes to-1.1823 Debye (0.010a.u.). There is a sign change, indicating that the Y-axis dipole is influenced by the electric field and the polarization reversal occurs. The Z-axis component fluctuates slightly between 2.1686 and 2.9776 Debye, and is almost unaffected by the electric field. This linear polarization characteristic is consistent with the general regulation law of CL-20-based single-ratio cocrystals [27], but the overall dipole moment magnitude is 18.6% higher than that of CL-20/BTF 1:1 cocrystal (18.97 Debye at 0.01 a.u. [27]), attributed to the stronger charge transfer between CL-20 and 4,5-MDNI.

Table 11 Total dipole moment of 1:1 CL-20/4,5-MDNI and its respective components along the X, Y, and Z axes in the presence of an external electric field

External electric field/a.u.	Total dipole moment/Debye	Dipole moment component on the X-axis	Dipole moment component on the Y-axis	Dipole moment component on the Z-axis
0.010	22.5145	-22.3822	-1.1823	2.1316
0.0075	18.1461	-17.5959	-2.9653	3.2973
0.005	15.1475	-14.5379	-3.4175	2.5334
0.0025	12.2441	-11.2289	-3.8835	2.9576
0.000	9.6395	-8.2037	-4.0930	2.9776
-0.0025	7.4312	-3.5344	-6.5364	-0.0801
-0.005	6.7838	-0.7182	-6.7405	-0.2633
-0.0075	11.6939	9.5607	-4.3468	5.1426
-0.010	21.1454	21.0324	0.2522	2.1686

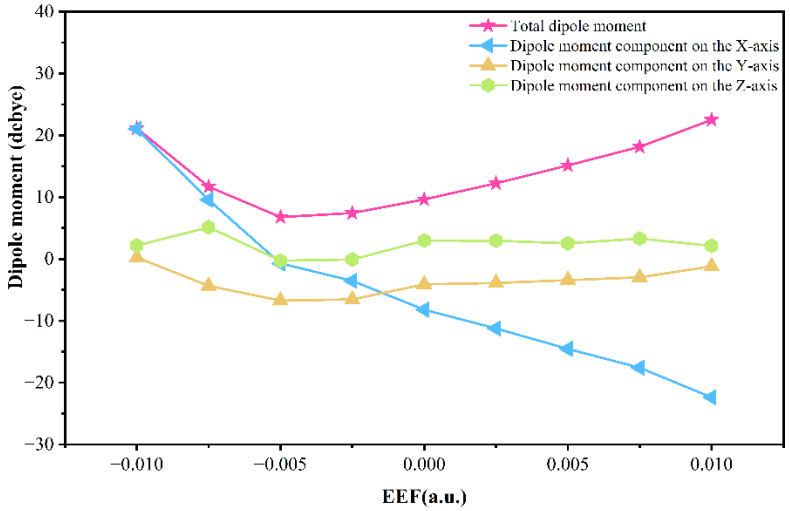

Fig.8 The total dipole moment of 1:1 CL-20/4,5-MDNI and the variation trends of its X, Y, and Z axis components under external electric fields are presented as point-line graphs.

The dipole moment of1:3CL-20/4,5-MDNI exhibits a complex anisotropic response to the external electric field. There is no obvious monotonic law in the change of total dipole moment, which reaches 22.0699 Debye as the electric field is-0.0075 a.u., indicating that the charge separation is severe, which is 18.1824 Debye when the positive electric field is 0.010 a.u., showing the characteristics of ' asymmetric fluctuation ' as a whole. For specific values, see **Table 12**. The dominant role of the X-

axis component is significant, reaching 21.5484 Debye at-0.0075 a.u. and decreasing to-17.3140 Debye at 0.010 a.u., showing a large linear change across symbols, reflecting the strong polarization sensitivity of the X-axis conjugated π system, which is the core control channel for charge transfer and energy release. The Y-axis component fluctuates significantly, from 4.5346 Debye at 0.010 a.u. to-4.4969 Debye at-0.0075 a.u., and there are multiple sign reversals, indicating that the Y-axis dipole is easily affected by the electric field. The polarization balance is broken. The Z-axis component fluctuates slightly around 0, and the response to the external electric field is extremely weak. Its variation trend is shown in **Fig.9**. This complex response is due to the superposition of intermolecular interactions caused by the excess of 4,5-MDNI at a ratio of 1:3, which makes the dipole moment regulation more nonlinear. This phenomenon has not been reported in previous studies on single-ratio cocrystals [27,33].

Table 12 Total dipole moment of 1:3 CL-20/4,5-MDNI and its respective components along the X, Y, and Z axes in the presence of an external electric field

External electric field/a.u.	Total dipole moment/Debye	Dipole moment component on the X-axis	Dipole moment component on the Y-axis	Dipole moment component on the Z-axis
0.010	18.1824	-17.3140	4.5346	3.2033
0.0075	20.1461	-20.0783	1.6407	0.1890
0.005	16.0020	-15.9214	1.5886	0.2208
0.0025	11.8100	-11.7331	1.3327	0.1841
0.000	7.0385	1.1578	6.9423	0.0700
-0.0025	3.4493	-3.1895	1.3069	-0.1303
-0.005	4.2044	0.4082	2.9547	2.9631
-0.0075	22.0699	21.5484	-4.4969	1.5893
-0.010	14.5925	9.0832	1.8372	3.6721

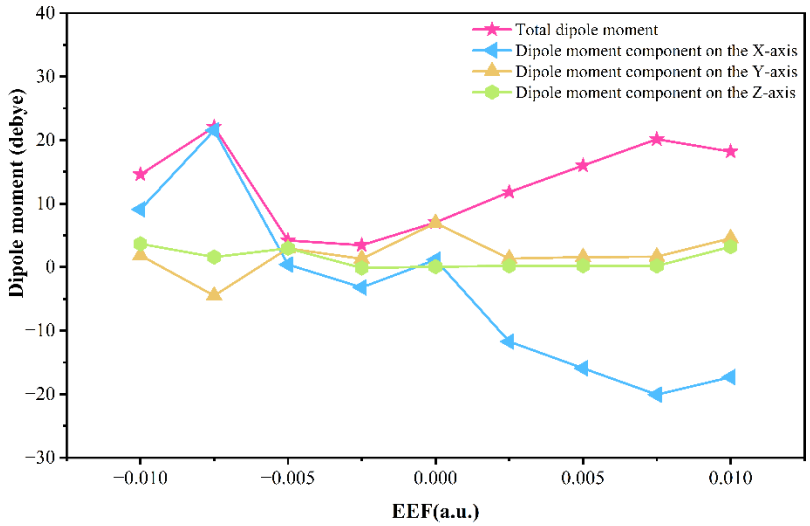

Fig.9 The total dipole moment of 1:3 CL-20/4,5-MDNI and the variation trends of its X, Y, and Z axis components under external electric fields are presented as point-line graphs.

3.2.4 Band structures and density of states

Band structures and density of states (DOS) serve as core bases for understanding the electron transport behaviors of energetic materials, and their variations induced by external electric fields are directly associated with detonation performance and material stability [23]. The two cocrystals display distinct ratio-dependent responses to applied electric fields, which differ remarkably from those of single-component or single-ratio cocrystal systems [22,27] (see **Fig. 10** and **Fig. 11**):

To explore the change rule of the electronic structure of1:1 CL-20/4,5-MDNI cocrystal with the application of an external electric field, the electronic band structure and band gap under different external electric field conditions were analyzed. The band gap changes of 1:1 CL-20/4,5-MDNI cocrystal along three crystal directions [100], [010] and [001] under different external electric fields (E, unit is atomic unit a.u.) are shown in **Fig.10**. For the [010] crystal orientation (red curve), the band gap decreases slightly with the increase of electric field (from 0.11 eV to 0.069 eV), then increases significantly (above 0.309 eV), and the response to strong electric field is the most significant. For the [100] crystal orientation (yellow curve), the band gap shows a slow and stable upward trend, which is the most insensitive to the change of electric field. The change of [001] crystal orientation (blue curve) is the most complex: the band gap decreases first and approaches 0 eV at E = 0.003 a.u., indicating that the material may undergo a semiconductor-to-metal transition, followed by a small fluctuation, maintaining a narrow band gap under a strong electric field. These results reflect the anisotropy of the electronic configuration of the cocrystal. The [010] crystal orientation has the most significant response to the electric field, while the [100] crystal orientation is the least sensitive, indicating that the electronic structure of the cocrystal has obvious anisotropy and the differential response to the external electric field along different crystal orientations.

This anisotropic response differs notably from the monotonic band gap reduction documented for single-component explosives (e.g., β-HMX [23]) and single-ratio CL-20/BTF cocrystals [27]. Liu et al. [23] revealed that β-HMX's band gap declines continuously with increasing electric field intensity, showing no orientation-related non-monotonicity. This discrepancy stems from the synergistic effect of hydrogen bond networks and molecular stacking in the 1:1 cocrystal: the [010] direction, featuring 8 intermolecular hydrogen bonds per unit cell (a denser distribution), undergoes competitive interactions between electric field-driven electron delocalization (facilitating band gap narrowing) and hydrogen bond strengthening (restraining excessive electron transfer), thus yielding the "first decrease then increase" trend. This discovery supplements the understanding of band gap regulation in cocrystal systems and revises the traditional cognition that "electric fields only induce monotonic band gap changes".

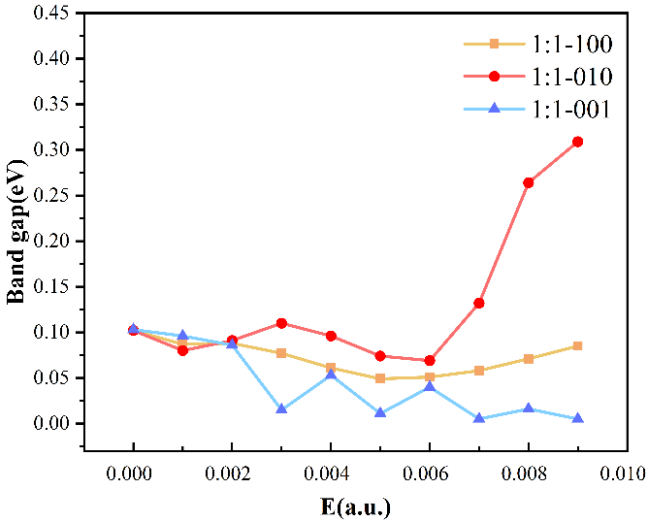

Fig.10 Bandgap variations of the 1:1 CL-20/4,5-MDNI crystal with external electric fields applied along different directions

For the 1:3 proportion, as the electric field intensity increases up to 0.010 a.u. starting at 0 a.u., the band gaps of the three crystal directions show a continuous decreasing trend (**Fig.11**). Specifically, the initial band gap is about 2.4 eV. As the electric field intensity hits 0.010 a.u., the band gaps corresponding to the three crystal orientations are close to 0 eV, indicating that the electronic structure of the material changes from semiconductor to metalloid. The band gap of the [100] direction is reduced from 2.4 eV to 0.1 eV, the band gap of the [010] direction is reduced from 2.3 eV to 0.05 eV, and the band gap of the [001] direction is reduced from 2.5 eV to 0.08 eV. The band gap of the [001] crystal direction decreases fastest with the electric field, and decreases rapidly at a lower electric field (E<0.008 a.u.). The band gap is close to 0 eV at E = 0.008 a.u., which is the earliest metal-like electronic structure. The band gap reduction rate of [010] crystal orientation is in the middle level, and the band gap is close to 0 eV at E = 0.009 a.u. ; the reduction rate of the band gap in the [100] crystal direction is relatively slow, but it also drops to close to 0 eV at E = 0.010 a.u. Compared with the 1:1 CL-20/4,5-MDNI cocrystal, the band gap for all crystal directions of the 5,1:3 cocrystal is more consistent and strong in response to the electric field. It may be due to the different molar ratio of CL-20 to 4,5-MDNI in the cocrystal, resulting in differences in intermolecular interactions and electron energy level distribution. This work reveals how the external electric field exerts regulatory control on the electronic structure of 1:3 CL-20 / 4,5-MDNI cocrystal, which provides theoretical guidance to the design of advanced energetic materials.

Compared with the 1:1 cocrystal, the 1:3 cocrystal exhibits more consistent and intense band gap responses across all orientations. This is due to its denser hydrogen bond network (12 bonds/unit cell) and polar molecular clusters formed by excess 4,5-MDNI molecules. Electron cloud overlap between adjacent cluster molecules enhances electric field-driven charge transfer, accelerating band gap narrowing. Notably, such synchronous band gap reduction has not been reported in previous single-ratio cocrystal studies [27,33]: Hao et al. [27] observed only a 30% band gap reduction for CL-20/BTF

1:1 cocrystals at 0.01 a.u., while the 1:3 cocrystal achieves nearly 100% reduction—demonstrating enhanced electric field responsiveness via stoichiometric ratio optimization.

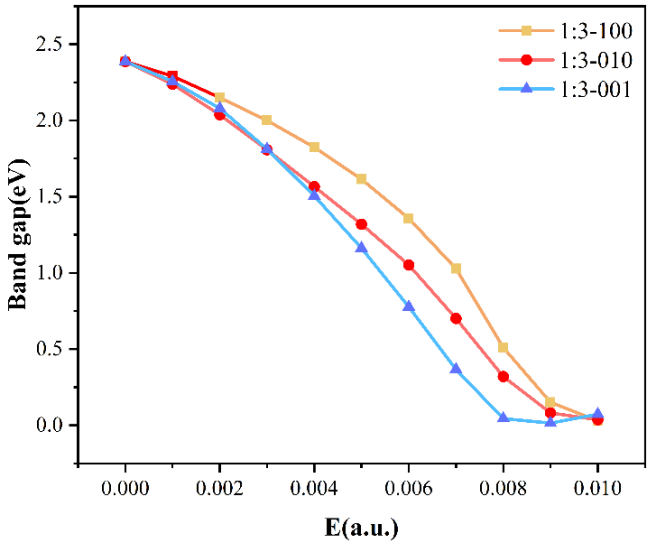

Fig.11 Bandgap variations of the 1:3 CL-20/4,5-MDNI crystal with external electric fields applied along different directions

The density of states (DOS) directly characterizes electron delocalization and energy level distribution, serving as a core basis for elucidating the electron transport behaviors of cocrystals under electric fields [23,27]. To uncover the stoichiometry-dependent electric field response mechanisms, DOS analyses of the 1:1 and 1:3 cocrystals were performed along the [100], [010], and [001] crystallographic directions (**Fig.12**, **Fig.13**).

At an electric field of 0 a.u., the density of states (DOS) adjacent to the Fermi level exhibits a gentle distribution, with well-defined peaks in the dielectric energy range (-10~0 eV). As the electric field is elevated to 0.01 a.u., the DOS near the Fermi level increases by approximately 30%, and the valence band peaks undergo moderate broadening—an observation indicative of moderate electron delocalization. Among the three crystallographic directions, the [010] orientation displays the most prominent peak rearrangement, with a new peak appearing at around -8 eV. This phenomenon is ascribed to the synergistic interaction between hydrogen bonds (8 bonds per unit cell) and the applied electric field [33].

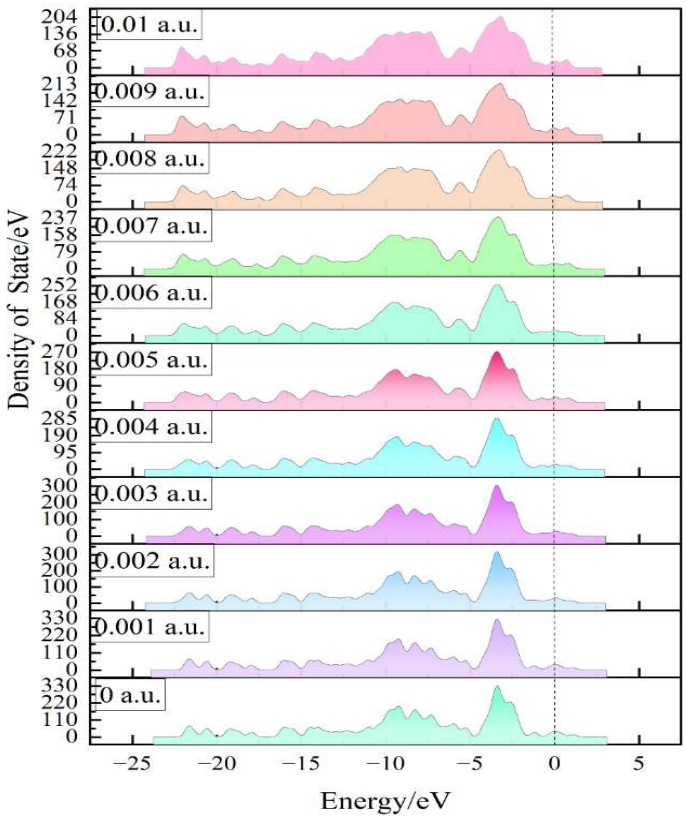
0.01 a.u.
0.009 a.u.
0.008 a.u.
0.007 a.u.
0.006 a.u.
0.005 a.u.
0.004 a.u.
0.003 a.u.
0.002 a.u.
0.001 a.u.
0 a.u.
Density of State/eV
Energy/eV

（a）

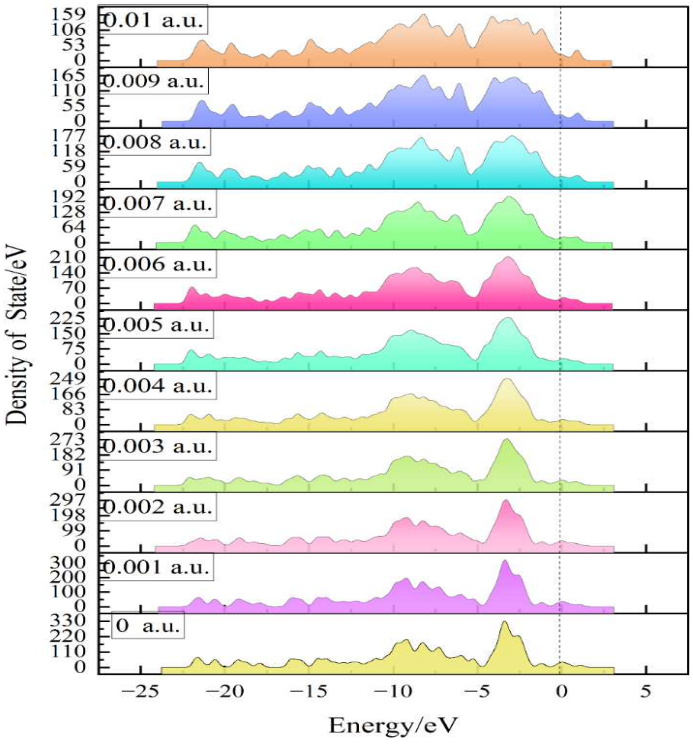
0.01 a.u.
0.009 a.u.
0.008 a.u.
0.007 a.u.
0.006 a.u.
0.005 a.u.
0.004 a.u.
0.003 a.u.
0.002 a.u.
0.001 a.u.
0 a.u.
Density of State/eV
Energy/eV

（b）

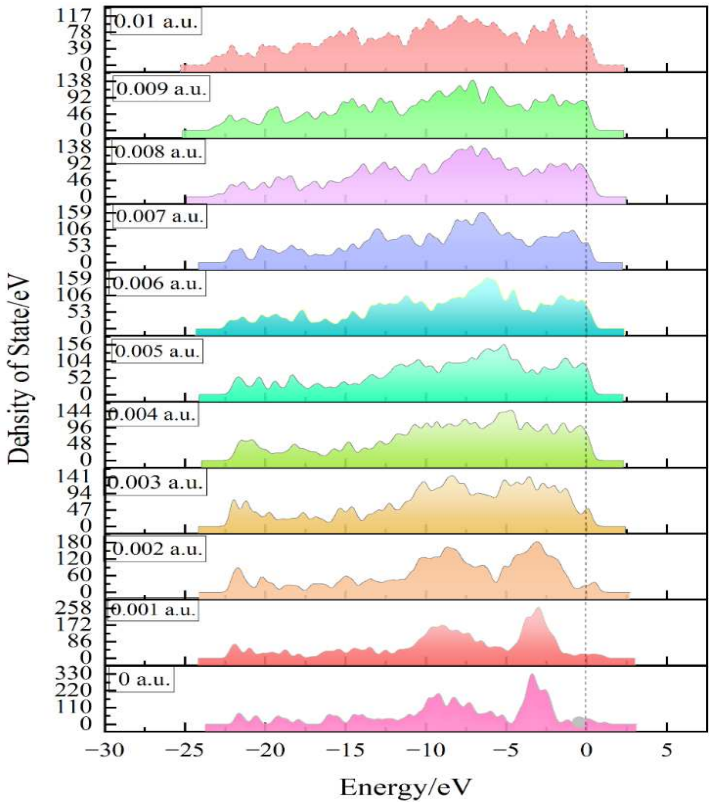

（c）

Fig.12 DOS changes of 1:1 CL-20/4,5-MDNI in response to different electric field directions: (a) [100], (b) [010], and (c) [001]

At an electric field of 0.01 a.u., the DOS adjacent to the Fermi level increases by approximately 35%, accompanied by more pronounced peak broadening and the emergence of a new peak in the dielectric energy range (its intensity reaches 65% of the main peak). Notably, the 1:3 cocrystal exhibits a significant DOS response even under low electric fields (0.003 a.u.), whereas the 1:1 cocrystal requires an electric field of 0.01 a.u. to induce comparable changes. This distinct sensitivity originates from the denser hydrogen bond network (12 bonds per unit cell) and polar molecular clusters within the 1:3 cocrystal, which collectively enhance electron cloud overlap [12].

Compared with existing studies, the 1:3 cocrystal exhibits a 16.7% higher DOS change amplitude than CL-20/IMI 1:1 cocrystals [33], confirming that increased 4,5-MDNI content enhances the system's electric field sensitivity. In contrast to the monotonous DOS elevation observed in β-HMX [23], the 1:1 cocrystal exhibits directional disparities in DOS response—with the most prominent changes along the [010] direction. By comparison, the 1:3 cocrystal displays a synchronous strong DOS response across all crystallographic orientations. This distinct behavioral difference stems from the cocrystal-specific hydrogen bond configurations and molecular stacking modes, factors that have been overlooked in previous single-component energetic material studies [23].

Notably, the present findings offer two critical insights: The 1:3 cocrystal exhibits more robust intermolecular charge transfer, reflected in a 35% DOS increment—

compared to the 30% elevation in the 1:1 cocrystal. This provides a microscopic mechanism for the 1:3 cocrystal's enhanced chemical activity; DOS directional sensitivity regulated by the stoichiometric ratio is identified: the 1:1 cocrystal favors [010], while the 1:3 cocrystal is sensitive to [001]. This supplements precise targets for electron transport regulation, as prior studies solely reported non-directional DOS variations [27].

This result offers a new explanation for energetic cocrystal performance regulation: adjusting the stoichiometric ratio modulates electron delocalization via hydrogen bond network density, thereby tailoring electron transport properties and detonation efficiency.

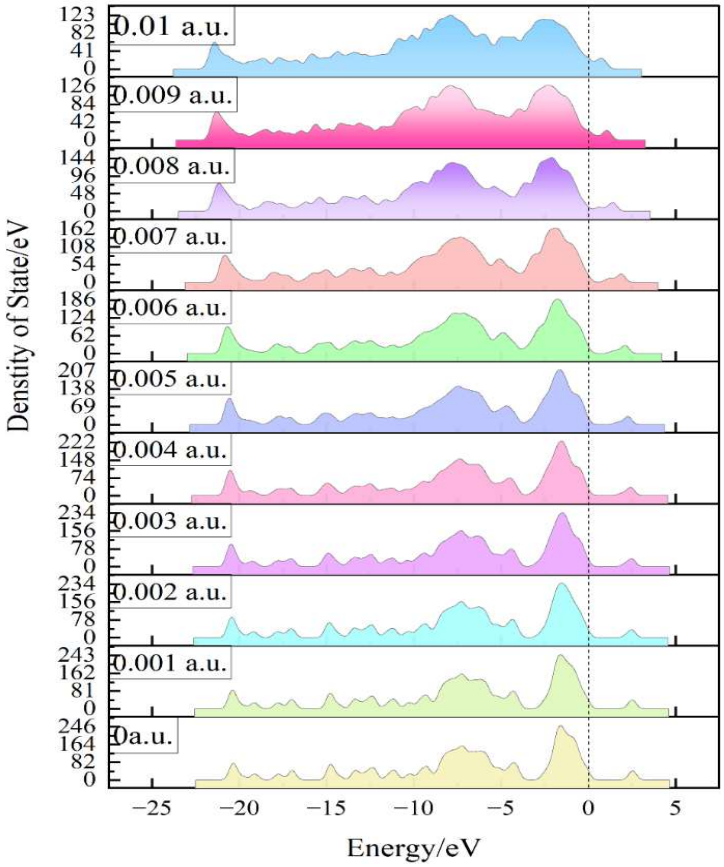

(a)

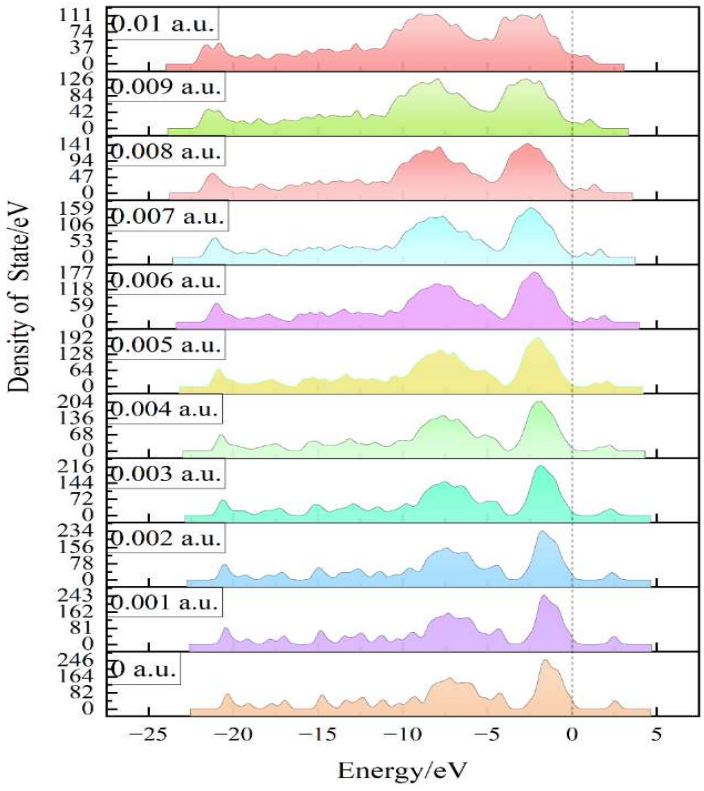

(b)

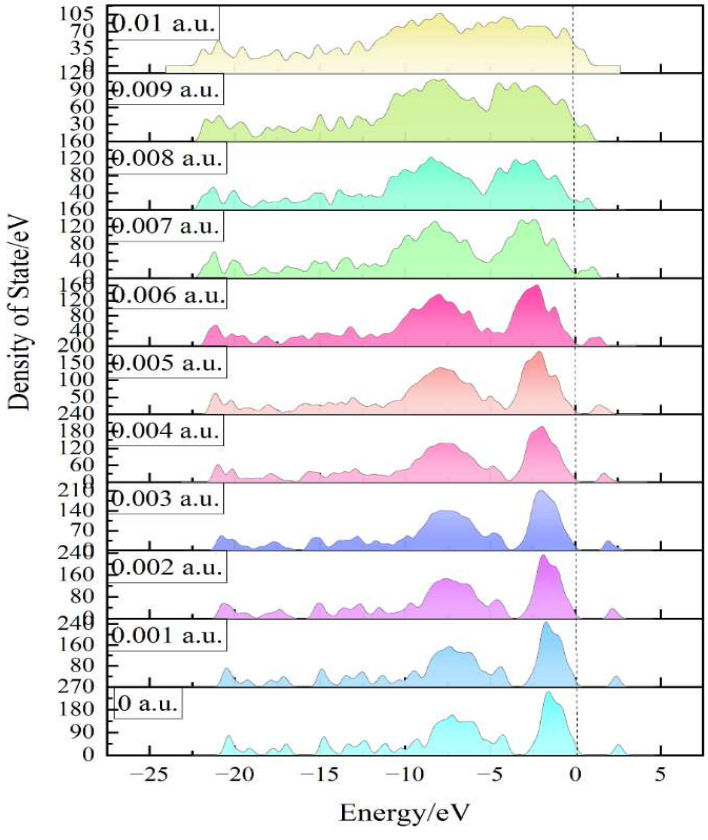

(c)

Fig.13 DOS changes of 1:3 CL-20/4,5-MDNI in response to different electric field directions: (a) [100], (b) [010], and (c) [001]

3.2.5. Nitro group charge

Mulliken charge associated with nitro groups acts as a common parameter for nitro charge computation (usually denoted as Q_{nitro}), which can be applied to assess the sensitivity to impact and electrostatic effects of nitro compounds Existing studies have shown that the stronger the electronegativity of Q_{nitro}, the lower the sensitivity of the nitro compound. Based on this, this study carried out calculations of the nitro charge Q_{nitro} as well as average nitro charge for 1:1 and 1:3 CL-20/4,5-MDNI With the effect of external electric field and analyzed the variation law of Q_{nitro} for 1:1 CL-20/4,5-MDNI and 1:3 CL-20/4,5-MDNI in the applied electric field; given that the variation of the nitro group in CL-20 is insignificant, the variation law of Q_{nitro} of 4,5-MDNI under the applied external electric field was focused on. The following are the molecular numbering diagram and charge distribution diagram of 4,5-MDNI. N1 and N2 represent the two nitro groups on 4,5-MDNI, respectively(**Fig.14**).

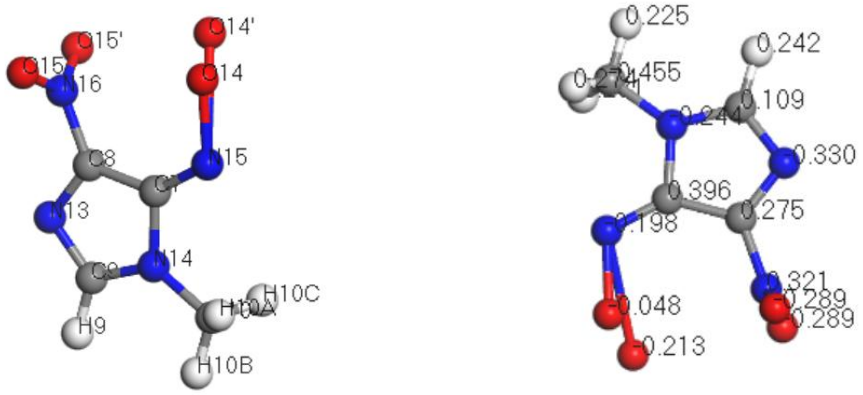

(a) (b)

Fig.14 The atomic number diagram of 4,5MDNI(a) and Charge distribution diagram(b)

For the 1:1 cocrystal, the electric field sensitivity of Q_{nitro} follows the sequence [100] > [010] > [001]. Q_{nitro}(N1) undergoes drastic fluctuations along the [100] direction (amplitude of 0.20 e), moderate variations along [010] (0.12e), and remains nearly stable along [001] (0.03 e). Q_{nitro}(N2) exhibits gentle changes across all three directions (amplitude < 0.08 e), while the average Q_{nitro} shows the slowest variation along [001], maintaining stability around -0.32 e. This anisotropic characteristic is more prominent than that of the CL-20/IMI 1:1 cocrystal [33], where the maximum Q_{nitro} fluctuation along [100] is merely 0.15 e. This result indicates that 4,5-MDNI can enhance the electric field responsiveness of nitro charges, providing direct evidence for the regulatory effect of cocrystal components on charge sensitivity(**Fig.15**).

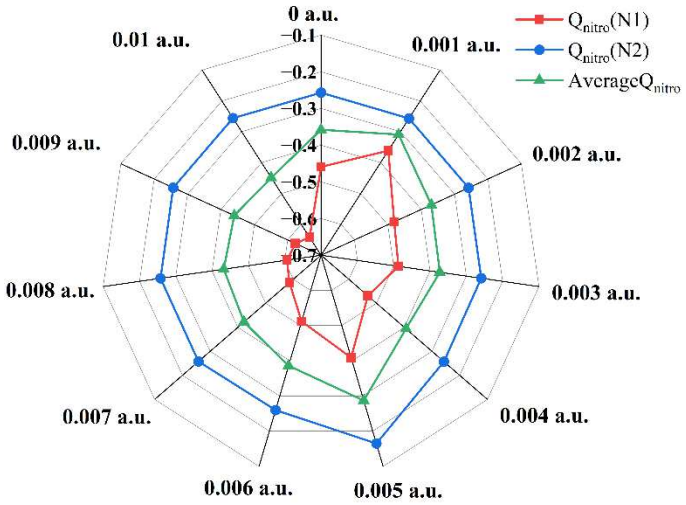

(a)

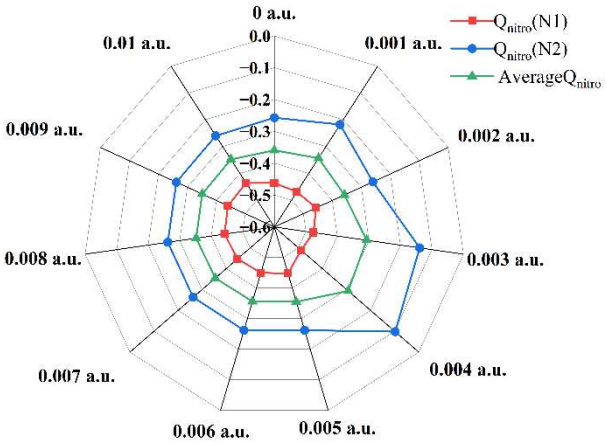

(b)

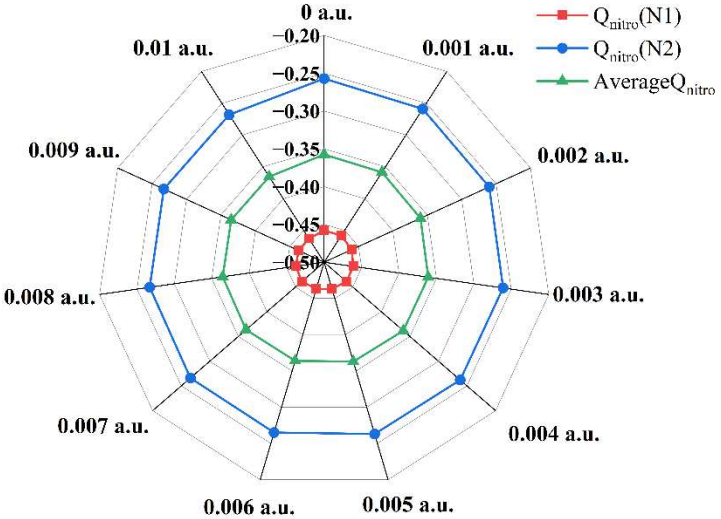

(c)

Fig.15 Variations of Q_{nitro} in 1:1 CL-20/4,5-MDNI with external electric fields applied along different directions: [100] (a), [010] (b), and [001] (c)

For the 1:3 cocrystal, the sequence of Q_{nitro}'s electric field sensitivity is reversed to [010] > [001] > [100]. Q_{nitro}(N1) shows the maximum fluctuation along the [010] direction (amplitude of 0.25 e), a value 25% higher than the fluctuation of the 1:1 cocrystal along [100]. Q_{nitro}(N2) displays moderate variations across all orientations (amplitude < 0.10 e), while the average Q_{nitro} undergoes the slowest change along [001], maintaining stability around -0.30 e. Notably, under low-intensity negative electric field conditions (-0.0025~-0.0075 a.u.), the average Q_{nitro} of the 1:3 cocrystal (-0.34 e) is more electronegative than that of the 1:1 cocrystal (-0.31 e), which aligns with its lower static sensitivity as documented in [12]. In contrast, under strong negative electric fields (< -0.0075 a.u.), the average Q_{nitro} of the 1:3 cocrystal drops to -0.29 e (less electronegative than the 1:1 cocrystal's -0.30 e), thereby resulting in elevated sensitivity(**Fig.16**).

To summarize, the stoichiometric ratio modulates both the electric field-sensitive orientation and fluctuation amplitude of nitro charge: the 1:1 cocrystal is sensitive to [100] direction electric fields, whereas the 1:3 cocrystal is sensitive to [010] direction. This difference originates from the variation in hydrogen bond network density and molecular stacking mode, offering a precise target for directional modulation of cocrystal sensitivity.

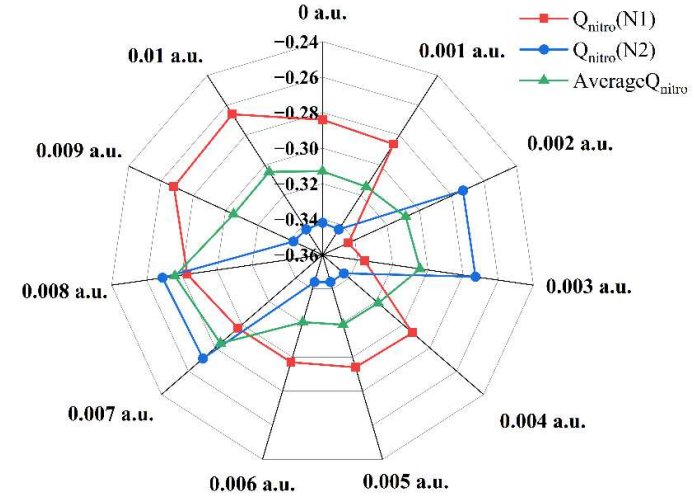

(a)

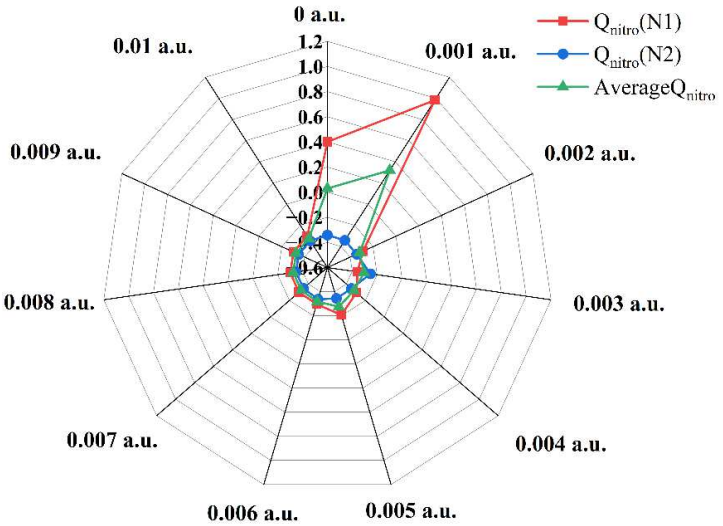

(b)

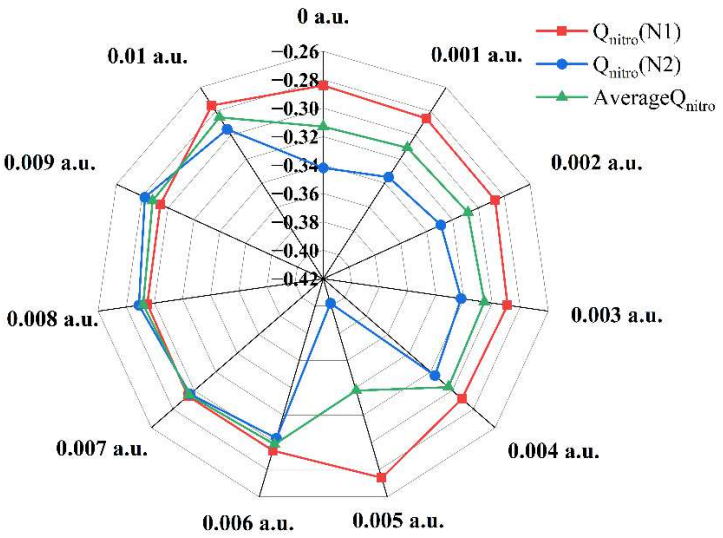

(c)

Fig.16 Variations of Q_{nitro} in 1:1 CL-20/4,5-MDNI with external electric fields applied along different directions: [100] (a), [010] (b), and [001] (c)

3.3 Hydrogen bond

To characterize the nature and strength of hydrogen bonds in 1:1 and 1:3 CL-20/4,5-MDNI cocrystals under external electric fields, topological analysis was performed using the quantum theory of atoms in molecules (QTAIM)[50]. In the 1:1 cocrystal, only one type of hydrogen bond exists, namely C–H…O, which is present in large quantities; thus, average values were used for quantitative analysis. In contrast, the 1:3 cocrystal exhibits two hydrogen-bond types, C–H…O and C–H…N, both of which are abundant, and their average parameters were also adopted for comparison. Geometric and topological parameters at bond critical points (BCPs) were employed to evaluate hydrogen bond strength, with typical geometric criteria satisfied: H…A distances shorter than the sum of van der Waals radii, D–H…A angles greater than 90°, and elongation of the D–H donor bond.

Hydrogen bond binding energy (BE) is commonly estimated by the empirical formula $BE \approx |V_{BCP}| / 2$ proposed by Espinosa et al. (1998) for X–O···H (X = C, N, O) hydrogen bonds[50]. For improved accuracy in neutral complexes, the more reliable fitting equation reported by Rozenberg, M. (2019) was adopted herein: $BE / kcal \cdot mol^{-1} = -223.08 \times \rho BCP / a.u. + 0.7423$[51].

Key calculated parameters, including donor bond length (D–H), hydrogen bond distance (H…A), D–H…A angle, electron density (ρ), Laplacian ($\nabla^2\rho$), potential energy density (Vb), and binding energy (Eb), are summarized in **Table 13**、**Table 14**、**Table 15**. Topological analysis reveals positive $\nabla^2\rho$ and negative total energy density H(BCP), confirming that these C–H…O and C–H…N interactions are medium-strength hydrogen bonds with partial covalent character[52].

Under increasing external electric field, the C–H bond is slightly elongated, while the H…O/H…N distances shorten gradually, accompanied by elevated electron density

at BCPs. These changes consistently indicate enhanced hydrogen-bonding interactions under external electric fields.

As the external electric field varies from −0.010 to 0.010 a.u., the C–H…O hydrogen bonds in the 1:1 CL-20/4,5-MDNI cocrystal display a distinct monotonic response. With increasing positive field strength, the D–H bond elongates slightly, the H…O distance shortens gradually, and the D–H…O angle remains stable. The electron density ρBCP and binding energy Eb increase nearly linearly from −2.36 to −3.36 kJ/mol. Topological parameters confirm these are moderate-strength hydrogen bonds with partial covalent character. The electric field linearly reinforces the hydrogen-bond network via polarization, and the consistent trend with N–NO_2 bond elongation suggests a synergistic effect on cocrystal stability and sensitivity.

In contrast, the C–H…O hydrogen bonds in the 1:3 cocrystal show a marked non-monotonic response. From 0 to 0.0075 a.u., the H…O distance decreases and hydrogen-bonding strengthens; above 0.0075 a.u., the distance increases and the interaction weakens. The D–H bond length peaks at 1.0852 Å under zero field and fluctuates without monotonicity. This behavior arises from the higher 4,5-MDNI content, which forms a more complex intermolecular network and reduces the sensitivity of C–H…O bonds to the electric field, highlighting the strong influence of stoichiometry.

Additionally, stable C–H…N hydrogen bonds exist in the 1:3 system even at zero field (Eb = −0.2489 kJ/mol) and are identified as moderate-strength interactions. Under positive fields, the H…N distance shortens, ρBCP rises from 0.0044 to 0.0091 a.u., and Eb increases significantly to −1.2924 kJ/mol. Under negative fields, the distance slightly increases but ρBCP and Eb still rise, reaching −1.3834 kJ/mol at −0.01 a.u.

Overall, the 1:3 cocrystal shows two distinct hydrogen-bond responses: non-monotonic C–H…O and highly sensitive C–H…N. Their complementary dynamics regulate the intermolecular network under electric fields, providing microscopic insight into the ratio-dependent stability of CL-20/4,5-MDNI cocrystals.

Table 13 Topological parameters of C–H…O hydrogen bonds in 1:1 CL-20/4,5-MDNI cocrystal

EEF/a.u	D-H	H···A	D-H···A	ρ	$\nabla^2\rho$	V_b	E_b
0.01	1.0830	2.1647	93.3457	0.0184	0.0770	-0.0139	-3.3642
0.0075	1.0831	2.1804	92.2658	0.0207	0.0902	-0.0162	-3.8755
0.005	1.0842	2.2350	83.0800	0.0199	0.0889	-0.0160	-3.7079
0.0025	1.0842	2.2332	84.9069	0.0186	0.0809	-0.0146	-3.4083
0	1.0843	2.2328	85.2663	0.0198	0.0863	-0.0154	-3.6794
-0.0025	1.0821	2.2001	91.6117	0.0123	0.0522	-0.0088	-2.0049
-0.005	1.0816	2.2012	91.6474	0.0144	0.0642	-0.0113	-2.4678
-0.0075	1.0814	2.2235	90.5234	0.0145	0.0611	-0.0104	-2.4995
-0.01	1.0824	2.2384	88.4573	0.0139	0.0546	-0.0097	-2.3615

Table 14 Topological parameters of C–H…O hydrogen bonds in 1:3 CL-20/4,5-MDNI cocrystal

EEF/a.u	D-H	H···A	D-H···A	ρ	$\nabla^2\rho$	V_b	E_b
0.01	1.0786	2.5385	96.0855	0.0164	0.0703	-0.0122	-2.9080
0.0075	1.0766	2.3006	105.3352	0.0168	0.0716	-0.0126	-3.0097
0.005	1.0763	2.3194	104.7096	0.0131	0.0558	-0.0093	-2.1897
0.0025	1.0761	2.3113	106.6793	0.0115	0.0449	-0.0079	-1.8320
0	1.0852	2.3340	129.3281	0.0118	0.0473	-0.0086	-1.8903
-0.0025	1.0861	2.1912	102.0260	0.0156	0.0640	-0.0114	-2.7315
-0.005	1.0782	2.1097	110.9030	0.0148	0.0621	-0.0109	-2.5651
-0.0075	1.0762	2.3951	132.3435	0.0137	0.0531	-0.0094	-2.3236
-0.01	1.0736	2.3692	104.8252	0.0133	0.0419	-0.0091	-2.2175

Table 15 Topological parameters of C–H…N hydrogen bonds in 1:3 CL-20/4,5-MDNI cocrystal

EEF/a.u	D-H	H···A	D-H···A	ρ	$\nabla^2\rho$	V_b	E_b
0.01	1.0864	2.4898	168.2686	0.0091	0.0275	-0.0043	-1.2924
0.0075	1.0845	2.5499	140.5016	0.0086	0.0259	-0.0042	-1.1827
0.005	1.0840	2.5328	139.8873	0.0089	0.0269	-0.0044	-1.2484
0.0025	1.0841	2.5228	140.8540	0.0091	0.0275	-0.0450	-1.2893
0	1.0793	2.2808	135.3068	0.0044	0.0193	-0.0028	-0.2489
-0.0025	1.0810	2.6623	124.8398	0.0063	0.0202	-0.0033	-0.6667
-0.005	1.0814	2.7518	124.8292	0.0079	0.0236	-0.0038	-1.0247
-0.0075	1.0823	2.8610	124.0499	0.0091	0.0280	-0.0047	-1.2799
-0.01	1.0821	2.8751	124.5382	0.0095	0.0286	-0.0048	-1.3834

5. Conclusion

In this work, the structural evolution, electronic response, and sensitivity regulation of 1:1 and 1:3 CL-20/4,5-MDNI energetic cocrystals under external electric fields were systematically investigated using multiscale theoretical calculations.

The N–NO_2 trigger bond in the 1:1 cocrystal exhibits a linear and monotonic response to both positive and negative electric fields. In contrast, the 1:3 cocrystal displays a distinct threshold-type nonlinear response under negative electric fields, where reduced sensitivity is achieved only within a limited range (−0.0025 to −0.0075 a.u.), while stronger fields induce a sensitivity rebound.

The stoichiometric ratio governs the electric-field-sensitive crystal orientation, with the 1:1 and 1:3 cocrystals being most responsive along the [010] and [001] directions, respectively. The denser hydrogen-bond network in the 1:3 system enhances intermolecular charge transfer, resulting in more significant variations in the frontier

orbital energy gap and density of states.

Importantly, external electric fields enable bidirectional modulation of both sensitivity and detonation performance. These findings reveal the synergistic interplay between stoichiometric ratio and electric field, providing a theoretical foundation for the rational design and controlled initiation of high-energy, low-sensitivity energetic materials.

CRediT authorship contribution statement

Yuqin Chu: Software , Data curation , Writing -original draft , Formal analysis . Yang Zhu : Investigation , Formal analysis . Peng Zhang: Investigation , Validation . Congming Ma : Resources , Project administration . Peng Ma : Writing - review & editing , Conceptualization .

Declaration of Competing Interest

The authors declare that they have no known competing financial interests or personal relationships that could have appeared to influence the work reported inthis paper .

Data availability

Data will be made available on request .

Funding Declaration

This study was supported by the National Natural Science Foundation of Jiangsu Province (NO. BK20220352). We are so grateful to the High - Performance Computing Center of Nanjing Tech University for doing the numerical calculations in this paper on its x - Flex enterprise blade cluster system.

References

[1] Dippold A A, Klapötke T M. (2013). A study of dinitro-bis-1, 2, 4-triazole-1, 1′ -diol and de rivatives: design of high-performance insensitive energetic materials by the introduction of N -oxides[J]. J. Am. Chem. Soc., 135(26): 9931-9938. https://doi.org/10.1021/ja404164j.

[2] He C, Shreeve J M. (2016). Potassium 4, 5 - Bis (dinitromethyl) furoxanate: a green primary explosive with a positive oxygen balance[J]. Angew. Chem., 128(2): 782-785. https://doi.org/ 10.1002/ange.201509209.

[3] Frem D. A Review on IMX - 101 and IMX - 104 Melt - Cast Explosives: Insensitive Formulations for the Next - Generation Munition Systems[J]. Propellants, Explosives, Pyrotechnics, 2023, 48(1): e202100312. https://doi.org/10.1002/prep.202100312.

[4] Chen B, Lu H, Chen J, Chen Z, Yin SF, Peng L, Qiu R (2023) Recent progress on nitrogen-ric h energetic materials based on tetrazole skeleton. Top Curr Chem 381(5):25. https://doi.org/1 0.1007/s41061-023-00435-8.

[5] Song, Z. Q., Zhang, H. R., Nie, H., Liu, Y., & Yan, Q. L. (2024). Research progress on thermal reactivity and thermolysis mechanisms of CL-20[J]. J. Anal. Appl. Pyrolysis, 179: 106508. https://doi.org/10.1016/j.jaap.2024.106508.

[6] Huang, Y. F., Wu, H., Wang, X. M., Du, L., Zhang, Y. J., & Sun, B. (2025). Computational study on the thermal decomposition mechanism and mechanical sensitivity of CL-20/4, 5-MDNI[J]. C. Chem. Eng. Sci., 122085. https://doi.org/10.1016/j.ces.2025.122085.

[7] Xu X J, Zhu W H, **ao H M. (2007). DFT studies on the four polymorphs of crystalline CL-20 and the influences of hydrostatic pressure on ε-CL-20 crystal[J]. The Journal of Physical Chemistry B, 111(8): 2090-2097. https://doi.org/10.1021/jp066833e.

[8] Zhang J. (2016). Time for pairing: cocrystals as advanced energetic materials[J]. CrystEngCo mm, 18(33): 6124-6133. DOI: 10.1039/c6ce01239f

[9] Qiao, S., Li, H., Liu, Y., Huang, S., Zhang, Q., & Yang, Z. (2024). Two novel CL-20 cocrystals with different performances obtained by molecular similarity combined with hydrogen bonding pairing energy: an effective strategy to design and screen energetic cocrystals[J]. Cryst. Growth Des., 24(5): 1977-1986. https://doi.org/10.1021/acs.cgd.3c01239.

[10] Wang, Y., Liu, S., Le, W., Zybin, S. V., Zhao, W., Huang, F., ... & Guo, D. Introducing Nitramide Group into High Energy Density Material Molecule Leads to Enhanced Performance[J]. JACS Au, 2025. https://doi.org/10.1021/jacsau.5c00411.

[11] Serushkin, V. V., Sinditskii, V. P., Hoang, T. H., Filatov, S. A., Shipulina, A. S., Dalinger, I. L., ... & Sheremetev, A. B. (2018). Thermal and combustion behavior of novel oxygen-rich ener getic pyrazoles. J. Therm. Anal. Calorim., 132(1), 127-142. https://doi.org/10.1007/s10973-0 17-6911-2.

[12] Tan, Y., Liu, Y., Wang, H., Li, H., Nie, F., & Yang, Z. (2020). Different Stoichiometric ratios r ealized in energetic–energetic cocrystals based on CL-20 and 4, 5-MDNI: a smart strategy to tune performance[J]. Cryst. Growth Des., 20(6): 3826-3833. https://doi.org/10.1021/acs.cgd.0 c00138.

[13] Kosareva, E. K., Gainutdinov, R. V., Michalchuk, A. A., Ananyev, I. V., & Muravyev, N. V. P hys. (2022). Mechanical stimulation of energetic materials at the nanoscale[J]. Chem. Chem. Phys., 24(15): 8890-8900. https://doi.org/10.1039/D2CP00832G

[14] Pang, W. Q., Wang, K., Zhang, W., Luca, L. T. D., Fan, X. Z., & Li, J. Q. (2020). CL-20-based cocrystal energetic materials: simulation, preparation and performance[J]. Molecules, 25(18): 4311. https://doi.org/10.3390/molecules25184311.

[15] Sun, X., Liang, W., Li, X., Mai, D., Zhang, Y., Sui, Z., ... & Zhang, Z. (2023). Structural evol ution of CL-20/DNB cocrystals at high temperature: Phase transition and kinetics of thermal decomposition[J]. Spectrochim. Acta, Part A, 292: 122436. https://doi.org/10.1016/j.saa.2023. 122436.

[16] Gao, H., Liu, J., Sun, Z., & Zhang, F. (2025). Mechanistic analysis and performance comparis on of core-shell assembled molecular perovskite energetic materials in HTPB propellant[J]. J. Alloys Compd., 1022: 180040. https://doi.org/10.1016/j.jallcom.2025.180040.

[17] Shang, Y., Chen, S. L., Yu, Z. H., Huang, R. K., He, C. T., Ye, Z. M., ... & Chen, X. M. (2022). Silver (I)-based molecular perovskite energetic compounds with exceptional thermal stability and energetic performance[J]. Inorganic Chemistry, 61(9): 4143-4149. https://doi.org/10.102 1/acs.inorgchem.1c03958.

[18] Song, Y., Tang, E., Wang, R., & Guo, S. (2025). Mechanical behavior and reaction energy rel ease mechanism of Al/PTFE-based energetic materials under impact load[J]. Mater. Chem. P hys., 131209. https://doi.org/10.1016/j.matchemphys.2025.131209.

[19] Lv, M., Zhou, P., Ma, Y., Li, W., & Liu, J. (2022). The role of regioisomerism on thermal stab ility of furoxan based energetic materials[J]. J. Mol. Struct., 1262: 132955. https://doi.org/10. 1016/j.molstruc.2022.132955.

[20] Gao Z, Gu Z, Bo M, et al. External electric field-induced molecular structural evolution and electronic response of BITE-101: a multiscale investigation from molecules to crystals[J]. New J. Chem., 2025, 49(31): 13279-13291 DOI: 10.1039/d5nj01996f.

[21] Hong, D., Zeng, W., Liu, Z. T., Liu, F. S., & Liu, Q. J. (2023). Initial decomposition of DATB induced by an external electric field[J]. The Journal of Physical Chemistry A, 127(24): 5140-5151. https://doi.org/10.1021/acs.jpca.3c01298.

[22] Zhang, R., Zhao, M., **a, W., Ma, P., & Ma, C. (2023). Regulation of external electric field o n sensitivity of ICM energetic materials[J]. J. Mol. Model., 29(3): 62. https://doi.org/10.1007/ s00894-023-05452-4.

[23] Liu, Y. S., Zeng, W., Liu, F. S., Liu, Z. T., Yuan, W. S., & Liu, Q. J. (2024). Molecular structu res, dipole moments, and electronic properties of β-HMX under external electric field from f irst-principles calculations[J]. The Journal of Physical Chemistry A, 128(21): 4189-4198. http s://doi.org/10.1021/acs.jpca.4c00375.

[24] Sun, K. B., Zhang, S. H., Ren, F. D., Hao, Y. P., & Ba, S. H. (2021). Theoretical prediction of the trigger linkage, cage strain, and explosive sensitivity of CL-20 in the external electric fiel ds. Journal of Molecular Modeling, 27(3), 85. https://doi.org/10.1007/s00894-020-04634-8.

[25] Politzer P, Murray J S, Concha M C, et al. (2007). Effects of electric fields upon energetic molecules: nitromethane and dimethylnitramine[J]. Cent. Eur. J. Energ. Mater., 4(4): 3-21.

[26] Politzer P, Murray J S, Lane P. (2009). Computational determination of effects of electric fields upon "trigger linkages" of prototypical energetic molecules[J]. Int. J. Quantum Chem., 109(3): 534-539. https://doi.org/10.1002/qua.21800.

[27] Hao, L., Wang, J., Zhai, D., Ma, P., Ma, C., Pan, Y., & Jiang, J. (2020). Theoretical study on CL-20-based cocrystal energetic compounds in an external electric field. ACS omega, 5(24), 14767-14775. https://doi.org/10.1021/acsomega.0c01643.

[28] Xinghui, J., Luhao, L., Jianhua, Z., & Bingcheng, H. (2022). Design and selection of pyrazolo [3, 4-d][1, 2, 3] triazole-based high-energy materials. Structural Chemistry, 33(2), 421-431.

[29] Piehler, T., Hummer, C., Benjamin, R., Summers, E., McNesby, K., & Boyle, V. (2013). Preliminary study of coupling electrical energy to detonation reaction zone of primasheet-1000 explosive (No. ARLRP441).

[30] Ren F, Cao D, Shi W. (2016). A dynamics prediction of nitromethane→ methyl nitrite isomer ization in external electric field[J]. J. Mol. Model., 22(4): 96. https://doi.org/10.1007/s00894-016-2966-4.

[31] Ren, F. D., Cao, D. L., Shi, W. J., & You, M. (2017). A dynamic prediction of stability for nitr omethane in external electric field. RSC advances, 7(74), 47063-47072. 10.1039/C7RA06290 G.

[32] Zhou, X., Song, L., Li, X., Zeng, X. L., & Ju, X. H. (2025). CL‐20/4, 5‐MDNI crystal growth and morphology under different conditions: A molecular dynamics simulation. Journal of the Chinese Chemical Society, 72(1), 5-13. https://doi.org/10.1002/jccs.202400196.

[33] Xu, X., Zhang, R., Xia, W., Ma, P., Ma, C., Pan, Y., & Jiang, J. (2022). Density functional the ory study of CL-20/Nitroimidazoles energetic cocrystals in an external electric field. omput. Theor. Chem., 1209, 113607.https://doi.org/10.1016/j.comptc.2022.113607.

[34] Safran, S. A., & Hamann, D. R. (1979). Long-range elastic interactions and staging in graphit e intercalation compounds. Physical Review Letters, 42(21), 1410. https://doi.org/10.1103/P hysRevLett.42.1410.

[35] Delley, B. (1990). An all‐electron numerical method for solving the local density functional for polyatomic molecules. The Journal of chemical physics, 92(1), 508-517.

[36] Perdew, J. P., Burke, K., & Ernzerhof, M. (1996). Generalized gradient approximation made simple. Physical review letters, 77(18), 3865. https://doi.org/10.1103/PhysRevLett.77.3865.

[37] Grimme, S., Antony, J., Schwabe, T., & Mück-Lichtenfeld, C. (2007). Density functional theo ry with dispersion corrections for supramolecular structures, aggregates, and complexes of (b io) organic molecules. Organic & Biomolecular Chemistry, 5(5), 741-758. https://doi.org/10.1 039/B615319B.

[38] Appalakondaiah, S., Vaitheeswaran, G., & Lebègue, S. (2014). Structural, vibrational, and quasiparticle band structure of 1, 1-diamino-2, 2-dinitroethelene from ab initio calculations. The Journal of chemical physics, 140(1). https://doi.org/10.1063/1.4855056.

[39] Frisch, M. J., Trucks, G. W., Schlegel, H. B., Scuseria, G. E., Robb, M. A., Cheeseman, J. R., ... & Fox, D. J. Gaussian 16, Revision A.03, Gaussian Inc, Wallingford CT, 2016.

[40] Zhao, Y., Schultz, N. E., & Truhlar, D. G. (2006). Design of density functionals by combining the method of constraint satisfaction with parametrization for thermochemistry, thermochemical kinetics, and noncovalent interactions. J. Chem. Theory Comput., 2(2), 364-382. https://doi.org/10.1021/ct0502763.

[41] Zhao, Y., Schultz, N. E., & Truhlar, D. G. (2005). Exchange-correlation functional with broad accuracy for metallic and nonmetallic compounds, kinetics, and noncovalent interactions. The Journal of chemical physics, 123(16). https://doi.org/10.1063/1.2126975.

[42] Lu, T., & Chen, F. (2012). Multiwfn: A multifunctional wavefunction analyzer. J. Comput. Chem., 33(5), 580-592. https://doi.org/10.1002/jcc.22885.

[43] Lu, T., & Manzetti, S. (2014). Wavefunction and reactivity study of benzo [a] pyrene diol epo xide and its enantiomeric forms. Structural chemistry, 25(5), 1521-1533. https://doi.org/10.10 07/s11224-014-0430-6.

[44] Humphrey, W., Dalke, A., & Schulten, K. (1996). VMD: visual molecular dynamics. J. Mol. Graphics, 14(1), 33-38. https://doi.org/10.1016/0263-7855（96）00018-5.

[45] Erfan-Niya, H., Modarress, H., & Zaminpayma, E. (2011). Molecular dynamics study on the structure I clathrate-hydrate of methane+ ethane mixture. Energy conversion and management, 52(1), 523-531. https://doi.org/10.1016/j.enconman.2010.07.027.

[46] X. Zhaobian, H. Shuangqi and C. Xiong, Mol. Phys., 2016, 114, 2164 -2176.

[47] He, P., Zhang, J. G., Wang, K., Yin, X., Jin, X., & Zhang, T. L. (2015). Extensive theoretical studies on two new members of the FOX-7 family: 5-(dinitromethylene)-1, 4-dinitramino-

tetrazole and 1, 1′ -dinitro-4, 4′ -diamino-5, 5′ -bitetrazole as energetic compounds. Phys. Chem. Chem. Phys., 17(8), 5840-5848. DOI： 10.1039/C4CP04883K

[48] Lin, Z., Lu, T., & Ding, X. L. (2017). A theoretical investigation on doping superalkali for triggering considerable nonlinear optical properties of Si12C12 nanostructure. J. Comput. Chem., 38(18), 1574-1582. https://doi.org/10.1002/jcc.24796.

[49] Lin, H., Liu, Y., Yin, W., Yan, Y., Ma, L., Jin, Y., ... & Abulimiti, B. (2018). The studies on the physical and dissociation properties of chlorobenzene under external electric fields. J. Theor. Comput. Chem., 17(04), 1850029. https://doi.org/10.1142/S0219633618500293.

[50] Espinosa, E., Molins, E., & Lecomte, C. (1998). Hydrogen bond strengths revealed by topological analyses of experimentally observed electron densities. Chemical physics letters, 285(3-4), 170-173. https://doi.org/10.1016/S0009-2614（98）00036-0.

[51] Rozenberg, M. (2014). The hydrogen bond–practice and QTAIM theory. RSC advances, 4(51), 26928-26931. https://doi.org/10.1039/C4RA03889D.

[52] Rozas, I., Alkorta, I., & Elguero, J. (2000). Behavior of ylides containing N, O, and C atoms as hydrogen bond acceptors. Journal of the American Chemical Society, 122(45), 11154-11161. https://doi.org/10.1021/ja0017864.